Commun. Appl. Math. Comput.
https://doi.org/10.1007/s42967-023-00307-4

ORIGINAL PAPER

A New Class of Simple, General and Efficient Finite Volume Schemes for Overdetermined Thermodynamically Compatible Hyperbolic Systems

Saray Busto[1] · **Michael Dumbser**[2]

*This paper is dedicated to Rémi Abgrall at the occasion of his 60*th *birthday and in honour of his groundbreaking scientific contributions to the field of numerical methods for hyperbolic PDE. The key ingredients of the numerical scheme presented in this paper are indeed based on the ideas and the work of Rémi Abgrall. The authors are also very grateful for the friendship and all the inspiring discussions.*

Received: 30 January 2023 / Revised: 30 May 2023 / Accepted: 15 August 2023

Abstract

In this paper, a new efficient, and at the same time, very simple and general class of thermodynamically compatible finite volume schemes is introduced for the discretization of nonlinear, overdetermined, and thermodynamically compatible first-order hyperbolic systems. By construction, the proposed semi-discrete method satisfies an entropy inequality and is nonlinearly stable in the energy norm. A very peculiar feature of our approach is that entropy is discretized directly, while total energy conservation is achieved as a mere consequence of the thermodynamically compatible discretization. The new schemes can be applied to a very general class of nonlinear systems of hyperbolic PDEs, including both, conservative and non-conservative products, as well as potentially stiff algebraic relaxation source terms, provided that the underlying system is overdetermined and therefore satisfies an additional extra conservation law, such as the conservation of total energy density. The proposed family of finite volume schemes is based on the seminal work of Abgrall [1], where for the first time a completely general methodology for the design of thermodynamically compatible numerical methods for overdetermined hyperbolic PDE was presented. We apply our new approach to three particular thermodynamically compatible systems: the equations of ideal magnetohydrodynamics (MHD) with thermodynamically compatible generalized Lagrangian multiplier (GLM) divergence cleaning, the unified first-order hyperbolic model of continuum mechanics proposed by Godunov, Peshkov, and Romenski (GPR model) and the first-order hyperbolic model for turbulent shallow water flows of Gavrilyuk et al. In addi-

✉ Michael Dumbser
michael.dumbser@unitn.it

Saray Busto
saray.busto@unitn.it

[1] Departamento de Matemática Aplicada I, Universidade de Vigo, Campus As Lagoas Marcosende s/n, E-36310 Vigo, Spain

[2] Department of Civil, Environmental and Mechanical Engineering, University of Trento, Via Mesiano 77, I-38123 Trento, Italy

tion to formal mathematical proofs of the properties of our new finite volume schemes, we also present a large set of numerical results in order to show their potential, efficiency, and practical applicability.

Keywords Overdetermined thermodynamically compatible hyperbolic systems · Hyperbolic and thermodynamically compatible (HTC) finite volume schemes · Abgrall framework · Discrete entropy inequality · Nonlinear stability in the energy norm · Applications to ideal magnetohydrodynamics (MHD), Godounov-Peshkov-Romenski (GPR) model of continuum mechanics · Turbulent shallow water (TSW) flows

Mathematics Subject Classification 35L40 · 65M08

1 Introduction

In his groundbreaking paper [43] from 1961 Godunov established for the first time, there was a rigorous mathematical connection between symmetric hyperbolicity in the sense of Friedrichs [37] and thermodynamic compatibility for overdetermined nonlinear systems of hyperbolic conservation laws. In [43], it was shown that for hyperbolic systems which have an underlying variational formulation, total energy conservation is a natural consequence of the governing PDE system, since the total energy conservation law can be obtained via a suitable linear combination of all other equations at the aid of the so-called main field or thermodynamic dual variables, which are the partial derivatives of the total energy potential with respect to the conservative variables. The terminology main field was introduced for the first time by Ruggeri and Strumia in [70], while in other papers, they are directly denoted as the Godunov variables, see e.g., [36]. The general formalism proposed by Godunov in his seminal work [43] was rediscovered independently 10 years later by Friedrichs and Lax in [38].

The formalism introduced by Godunov in [43] applies directly, for example, to the Euler equations of compressible gas dynamics and to other simple systems of hyperbolic conservation laws, but not to hyperbolic PDE with non-conservative products or to hyperbolic systems with involution constraints.

In subsequent works, Godunov and Romenski extended the ideas outlined in [43] to a more complete theory on general symmetric hyperbolic and thermodynamically compatible (SHTC) systems, which govern a rather wide class of mathematical models used in physics and engineering. Some examples of hyperbolic systems that fall into the general class of SHTC systems are: the equations of ideal magnetohydrodynamics (MHD), see [44], the equations of nonlinear hyperelasticity, see [46], the model of compressible multi-phase flows introduced and studied in [55, 66, 68, 74], continuum mechanics with torsion [61] and very recently it was shown that even relativistic fluid and solid mechanics can be rewritten within the SHTC framework, see e.g., [45, 67]. In [59], a connection between Hamiltonian continuum mechanics and the class of SHTC systems has been discovered. Very recently, a thermodynamically compatible hyperbolic reformulation of nonlinear dispersive systems based on an augmented Lagrangian approach has been obtained and studied numerically in [28, 29, 33]. For an overview and general introduction to the SHTC framework, the reader is referred to [64].

In SHTC systems, the PDE for the entropy density with non-negative right-hand side (second principle of thermodynamics) is usually the primary evolution variable, while total

energy conservation (first principle of thermodynamics) is typically the extra conservation law that is obtained as a consequence of all other equations via a suitable linear combination. All SHTC systems can be derived from an underlying variational principle and the total energy density has a privileged role because it directly appears inside the Lagrangian. Furthermore, as remarked in [3], in the Gibbs identity, the factor that multiplies the total energy differential is unity, while for all other equations, the factors are the Godunov variables.

All above considerations and mathematical properties apply to the overdetermined PDE system at the continuous level. From a numerical analysis point of view, it is now very interesting to develop numerical schemes that are also thermodynamically compatible at a discrete level, in such a way that a discrete extra conservation law is a consequence of a compatible discretization of the underlying governing PDE system. The standard approach consists of developing numerical schemes for which the entropy inequality is a consequence of the equations, while total energy is discretized directly. These so-called entropy preserving or provably entropy-stable schemes are based on the seminal work of Tadmor [72]. Very important contributions to the development of high-order entropy-compatible schemes can be found, e.g., in the papers of Mishra et al. [20, 35, 50], Gassner et al. [27, 40, 49, 69, 71], Shu et al. [25, 54], and in [21–23, 39, 62, 63] and references therein. Entropy-compatible schemes for hyperbolic PDE with non-conservative products were presented for the first time in [34].

Very recently, in [1, 2, 4], Abgrall and collaborators have forwarded a very simple, efficient and totally general framework that allows the construction of thermodynamically compatible schemes for overdetermined hyperbolic PDE systems. These schemes are able to satisfy an extra conservation law at the discrete level by construction. Hence, they will be used as starting point for the new thermodynamically compatible finite volume method for overdetermined systems introduced in this paper. The main difference is, however, that in the schemes presented in this paper, the total energy conservation law is obtained as a consequence, while in the previously mentioned references, the total energy density was discretized as a primary variable, as in traditional entropy-compatible schemes.

Numerical schemes which directly discretize the entropy inequality and which are able to obtain the total energy conservation law as a mere consequence of the compatible discretization of all the other equations of the overdetermined system are up to now still quite rare. Some progress in this direction has been recently made in [3, 15–17]. There is a new class of thermodynamically compatible finite volume schemes which have been introduced for the Euler equations of compressible gasdynamics, for the equations of ideal MHD, for the hyperbolic model of turbulent shallow water flows of Gavrilyuk et al. and for the unified model of continuum mechanics of Godunov, Peshkov, and Romenski (GPR model). In [15, 17], the entropy density was evolved as primary variable, while discrete total energy conservation was a mere consequence of the thermodynamically compatible finite volume discretization of the other equations. Very recently, these ideas have been extended to the discontinuous Galerkin (DG) framework in [3]. The methods presented in [15–17] have a path integral as common building block in order to obtain a thermodynamically compatible numerical flux. Inside the scheme, the path integral is then approximated at the aid of a suitable numerical quadrature formula. This approach is not only prone to quadrature errors, but is also computationally expensive, see [3]. Furthermore, in our previous schemes [3, 15–17], the non-conservative terms had to be judiciously discretized "by hand" and case by case in order to obtain a provably thermodynamically compatible scheme.

It is therefore the main objective of the present paper to construct thermodynamically compatible finite volume schemes for very general conservative and non-conservative overdetermined hyperbolic systems that do not need path integrals in order to obtain a thermodynamically compatible numerical flux and that are able to achieve a compatible

discretization of the non-conservative products automatically and not case by case. The finite volume schemes presented in this paper are therefore a further and natural generalization of the finite volume methods introduced in [3].

In order to show the generality of the new schemes proposed in this paper, in Sect. 2, we present the set of three rather different overdetermined hyperbolic PDE systems to be treated in this paper, namely the equation of ideal MHD with thermodynamically compatible generalized Lagrangian multiplier (GLM) divergence cleaning [15], the first order hyperbolic GPR model of continuum mechanics [30, 60, 64] and the first-order hyperbolic model of turbulent shallow water flows [16, 52]. The numerical scheme is presented and analyzed in Sect. 3. In Sect. 4, we show numerical results for a wide range of test cases for each of the three PDE systems and in Sect. 5, we draw the conclusions and give an outlook to possible future research.

2 Governing Equations

2.1 General Formulation

All overdetermined systems of nonlinear hyperbolic, thermodynamically compatible partial differential equations considered in this paper, i.e., the equations of ideal MHD recalled in (6), the unified first-order hyperbolic model of continuum mechanics of the GPR model presented in (11) and the hyperbolic model of turbulent shallow water (TSW) flows of Gavrilyuk et al. given by system (21), can be cast into the general form of a nonlinear hyperbolic system of balance laws with parabolic vanishing viscosity regularization,

$$\partial_t \mathbf{q} + \partial_k \mathbf{f}_k(\mathbf{q}) + \mathbf{B}_k(\mathbf{q})\partial_k \mathbf{q} - \partial_m \left(\epsilon \partial_m \mathbf{q}\right) = \mathbf{P} + \mathbf{S}(\mathbf{q}), \tag{1}$$

and they are all endowed with an extra conservation law for the total energy density of the form

$$\frac{\partial \mathcal{E}}{\partial t} + \partial_k F_k - \partial_m \left(\epsilon \partial_m \mathcal{E}\right) = 0. \tag{2}$$

Here, $\mathbf{q}$ is the state vector, the flux tensor is denoted by $\mathbf{f}_k(\mathbf{q})$, and $\mathbf{B}_k(\mathbf{q})\partial_k \mathbf{q}$ includes the non-conservative products. The parabolic regularization terms read $\partial_m \left(\epsilon \partial_m \mathbf{q}\right)$, with the vanishing viscosity parameter $\epsilon > 0$ and the associated entropy production term contained in $\mathbf{P}$. If present in the model, the (potentially stiff) algebraic relaxation source terms are contained in $\mathbf{S}(\mathbf{q})$. In the extra conservation law (2), the total energy flux is denoted by $F_k = F_k(\mathbf{q})$.

The main field or thermodynamic dual variables are defined as $\mathbf{p} = \partial_{\mathbf{q}} \mathcal{E}$ and therefore one trivially has $\mathbf{p} \cdot \partial_t \mathbf{q} = \partial_t \mathcal{E}$. Thus, for thermodynamic compatibility of the full system (1) with (2), the following identity must hold:

$$\mathbf{p} \cdot \partial_k \mathbf{f}_k(\mathbf{q}) + \mathbf{p} \cdot \mathbf{B}_k(\mathbf{q})\partial_k \mathbf{q} = \partial_k F_k. \tag{3}$$

Moreover, we also have

$$\mathbf{p} \cdot \mathbf{P} + \mathbf{p} \cdot \partial_m \left(\epsilon \partial_m \mathbf{q}\right) = \partial_m \left(\epsilon \partial_m \mathcal{E}\right), \tag{4}$$

i.e., the compatibility of the non-negative entropy production term with the dissipative parabolic vanishing viscosity terms. Finally, the relation

$$\mathbf{p} \cdot \mathbf{S}(\mathbf{q}) = 0 \tag{5}$$

is required for the thermodynamic compatibility of the algebraic source terms, if present in the system.

2.2 The MHD Equations with Compatible GLM Divergence Cleaning

As a first example of an overdetermined hyperbolic system, we consider a particular formulation of the equations of ideal MHD. The system is augmented with a novel hyperbolic and thermodynamically compatible GLM divergence cleaning introduced in [15], which is slightly different from the original GLM divergence cleaning introduced by Munz and collaborators in [26, 56]. Furthermore, the system also includes a parabolic vanishing viscosity regularization and reads

$$\frac{\partial \rho}{\partial t} + \frac{\partial (\rho v_k)}{\partial x_k} - \frac{\partial}{\partial x_m} \epsilon \frac{\partial \rho}{\partial x_m} = 0, \tag{6a}$$

$$\frac{\partial \rho v_i}{\partial t} + \frac{\partial \left(\rho v_i v_k + p\, \delta_{ik} + \frac{1}{2} B_m B_m \delta_{ik} - B_i B_k \right)}{\partial x_k} - \frac{\partial}{\partial x_m} \epsilon \frac{\partial \rho v_i}{\partial x_m} = 0, \tag{6b}$$

$$\frac{\partial \rho S}{\partial t} + \frac{\partial \left(\rho S v_k \right)}{\partial x_k} - \frac{\partial}{\partial x_m} \epsilon \frac{\partial \rho S}{\partial x_m} = \Pi \geqslant 0, \tag{6c}$$

$$\frac{\partial B_i}{\partial t} + \frac{\partial \left(B_i v_k - v_i B_k \right)}{\partial x_k} + v_i \frac{\partial B_k}{\partial x_k} + c_h \frac{\partial \varphi}{\partial x_i} - \frac{\partial}{\partial x_m} \epsilon \frac{\partial B_i}{\partial x_m} = 0, \tag{6d}$$

$$\frac{\partial \varphi}{\partial t} + v_k \frac{\partial \varphi}{\partial x_k} + \frac{c_h}{\rho} \frac{\partial B_k}{\partial x_k} - \frac{\partial}{\partial x_m} \epsilon \frac{\partial \varphi}{\partial x_m} = 0 \tag{6e}$$

with the extra conservation law

$$\frac{\partial \mathcal{E}}{\partial t} + \frac{\partial \left(\mathcal{E} v_k + v_i (p\, \delta_{ik} + \frac{1}{2} B_m B_m \delta_{ik} - B_i B_k) + c_h \varphi B_k \right)}{\partial x_k} - \frac{\partial}{\partial x_m} \epsilon \frac{\partial \mathcal{E}}{\partial x_m} = 0. \tag{7}$$

In the augmented MHD equations with thermodynamically compatible GLM divergence cleaning above the state vector is $\mathbf{q} = \{q_i\} = (\rho, \rho v_i, \rho S, B_i, \varphi)^{\mathrm{T}}$ with ρ the mass density, v_i the velocity, S the specific entropy, B_i the magnetic field, φ the GLM cleaning scalar, and the total energy density $\mathcal{E} = \rho E$ is a sum of four different contributions

$$\mathcal{E} = \rho E = \mathcal{E}_1 + \mathcal{E}_2 + \mathcal{E}_3 + \mathcal{E}_4 = \rho E_1 + \rho E_2 + \rho E_3 + \rho E_4$$

with $\mathcal{E}_i = \rho E_i$ and E the specific total energy. Furthermore, $\epsilon \geqslant 0$ is a vanishing viscosity coefficient, $c_h \geqslant 0$ is the divergence cleaning speed, the positive temperature is denoted by $T > 0$, and the non-negative entropy production term due to the vanishing viscosity regularization reads

$$\Pi = \frac{\epsilon}{T} \frac{\partial q_i}{\partial x_m} \partial^2_{q_i q_j} \mathcal{E} \frac{\partial q_j}{\partial x_m} \geqslant 0. \tag{8}$$

We assume that the Hessian matrix of the total energy density w.r.t. the vector of primary evolution variables is at least positive semi-definite, $\mathcal{H}_{ij} := \partial^2_{q_i q_j} \mathcal{E} \geqslant 0$. In the following, we make use of the notations $\partial_p = \frac{\partial}{\partial p}$ and $\partial^2_{pq} = \frac{\partial^2}{\partial p \partial q}$ for the first and second partial derivatives with respect to the quantities or coordinates p and q. We also use the Einstein summation convention over repeated indices. For convenience, we will also make use of bold face symbols to denote vectors, e.g., $\mathbf{q} = \{q_i\}$. The four contributions to the total energy density read

$$\mathcal{E}_1 = \frac{\rho^\gamma}{\gamma - 1} \mathrm{e}^{S/c_v}, \quad \mathcal{E}_2 = \frac{1}{2} \rho v_i v_i, \quad \mathcal{E}_3 = \frac{1}{2} B_m B_m, \quad \mathcal{E}_4 = \frac{1}{2} \rho \varphi^2, \tag{9}$$

hence the associated contributions E_i to the specific total energy E are $E_i = \frac{\mathcal{E}_i}{\rho}$. The vector of main field variables reads $\mathbf{p} = \mathcal{E}_{\mathbf{q}} = (r, v_i, T, \beta_i, \psi)^{\mathrm{T}}$ with

$$r = \partial_\rho \mathcal{E}, \quad v_i = \partial_{\rho v_i} \mathcal{E}, \quad T = \partial_{\rho S} \mathcal{E}, \quad \beta_i = \partial_{B_i} \mathcal{E}, \quad \psi = \partial_\varphi \mathcal{E}, \tag{10}$$

and the pressure is given by $p = \rho^2 \frac{\partial E}{\partial \rho}$, where E denotes the specific total energy.

2.3 Godunov-Peshkov-Romenski (GPR) Model of Continuum Mechanics

The next system is the unified hyperbolic model of continuum mechanics of the GPR model [30, 46, 47, 60, 64]. It reads

$$\frac{\partial \rho}{\partial t} + \frac{\partial (\rho v_k)}{\partial x_k} - \frac{\partial}{\partial x_m}\left(\epsilon \frac{\partial \rho}{\partial x_m}\right) = 0, \tag{11a}$$

$$\frac{\partial \rho v_i}{\partial t} + \frac{\partial \left(\rho v_i v_k + p\, \delta_{ik} + \sigma_{ik} + \omega_{ik}\right)}{\partial x_k} - \frac{\partial}{\partial x_m}\left(\epsilon \frac{\partial \rho v_i}{\partial x_m}\right) = 0, \tag{11b}$$

$$\frac{\partial \rho S}{\partial t} + \frac{\partial \left(\rho S v_k + \beta_k\right)}{\partial x_k} - \frac{\partial}{\partial x_m}\left(\epsilon \frac{\partial \rho S}{\partial x_m}\right) = \Pi + \frac{\alpha_{ik}\alpha_{ik}}{\theta_1(\tau_1) T} + \frac{\beta_i \beta_i}{\theta_2(\tau_2) T} \geqslant 0, \tag{11c}$$

$$\frac{\partial A_{ik}}{\partial t} + \frac{\partial (A_{im} v_m)}{\partial x_k} + v_m \left(\frac{\partial A_{ik}}{\partial x_m} - \frac{\partial A_{im}}{\partial x_k}\right) - \frac{\partial}{\partial x_m}\left(\epsilon \frac{\partial A_{ik}}{\partial x_m}\right) = -\frac{\alpha_{ik}}{\theta_1(\tau_1)}, \tag{11d}$$

$$\frac{\partial J_k}{\partial t} + \frac{\partial \left(J_m v_m + T\right)}{\partial x_k} + v_m \left(\frac{\partial J_k}{\partial x_m} - \frac{\partial J_m}{\partial x_k}\right) - \frac{\partial}{\partial x_m}\left(\epsilon \frac{\partial J_k}{\partial x_m}\right) = -\frac{\beta_k}{\theta_2(\tau_2)} \tag{11e}$$

with the additional total energy conservation law

$$\frac{\partial \mathcal{E}}{\partial t} + \frac{\partial \left(v_k \left(\mathcal{E}_1 + \mathcal{E}_2 + \mathcal{E}_3 + \mathcal{E}_4\right) + v_i \left(p\, \delta_{ik} + \sigma_{ik} + \omega_{ik}\right) + h_k\right)}{\partial x_k} - \frac{\partial}{\partial x_m}\left(\epsilon \frac{\partial \mathcal{E}}{\partial x_m}\right) = 0. \tag{12}$$

In the GPR model, the state vector is $\mathbf{q} = \{q_i\} = (\rho, \rho v_i, \rho S, A_{ik}, J_k)^{\mathrm{T}}$ with ρ the mass density, v_i the velocity, S the specific entropy, A_{ik} the distortion field, J_k the specific thermal impulse, and the total energy density is $\mathcal{E} = \rho E = \mathcal{E}_1 + \mathcal{E}_2 + \mathcal{E}_3 + \mathcal{E}_4$ with $\mathcal{E}_i = \rho E_i$. Furthermore, $\epsilon > 0$ denotes again the vanishing viscosity parameter and the associated non-negative entropy production reads

$$\Pi = \frac{\epsilon}{T}\, \partial_{x_m} q_i \;\, \partial^2_{q_i q_j} \mathcal{E}\, \partial_{x_m} q_j \geqslant 0. \tag{13}$$

We also introduce the following abbreviation:

$$\pi = \frac{\alpha_{ik}\alpha_{ik}}{\theta_1(\tau_1) T} + \frac{\beta_i \beta_i}{\theta_2(\tau_2) T} \geqslant 0 \tag{14}$$

for the contribution of the algebraic relaxation source terms to the entropy production. The four contributions to the total energy density are

$$\mathcal{E}_1 = \frac{\rho^\gamma}{\gamma - 1} \mathrm{e}^{S/c_v}, \quad \mathcal{E}_2 = \frac{1}{2} \rho v_i v_i, \quad \mathcal{E}_3 = \frac{1}{4} \rho c_s^2 \mathring{G}_{ij} \mathring{G}_{ij}, \quad \mathcal{E}_4 = \frac{1}{2} c_h^2 \rho J_i J_i \tag{15}$$

with the metric tensor $\mathbf{G}$ given by $G_{ik} = A_{ji} A_{jk}$ and its trace-free part $\mathring{\mathbf{G}}$ defined as $\mathring{G}_{ik} = G_{ik} - \frac{1}{3} G_{mm} \delta_{ik}$. The Godunov variables of the system are $\mathbf{p} = \partial_{\mathbf{q}} \mathcal{E} = \{p_i\} = (r, v_i, T, \alpha_{ik}, \beta_k)^{\mathrm{T}}$ with

$$r = \partial_\rho \mathcal{E}, \quad v_i = \partial_{\rho v_i} \mathcal{E}, \quad T = \partial_{\rho S} \mathcal{E}, \quad \alpha_{ik} = \partial_{A_{ik}} \mathcal{E}, \quad \beta_k = \partial_{J_k} \mathcal{E}. \tag{16}$$

The pressure is given by $p = \rho\,\partial_\rho \mathcal{E} + \rho v_i\,\partial_{\rho v_i}\mathcal{E} + \rho S\,\partial_{\rho S}\mathcal{E} - \mathcal{E} = \rho^2 \partial_\rho E$, while the stress tensors due to shear and thermal stress are, respectively,

$$\sigma_{ik} = A_{ji}\,\partial_{A_{jk}}\mathcal{E} = A_{ji}\alpha_{jk} = \rho c_s^2 G_{ij}\mathring{G}_{jk}, \quad \omega_{ik} = J_i\,\partial_{J_k}\mathcal{E} = J_i\beta_k = \rho c_h^2 J_i J_k. \tag{17}$$

The heat flux reads

$$h_k = \partial_{\rho S}\mathcal{E}\,\partial_{J_k}\mathcal{E} = T\beta_k = \rho c_h^2 T J_k. \tag{18}$$

The two functions $\theta_1(\tau_1) > 0$ and $\theta_2(\tau_2) > 0$ depend on $\mathbf{q}$ and on the relaxation times $\tau_1 > 0$ and $\tau_2 > 0$ as follows:

$$\theta_1 = \frac{1}{3}\rho z_1 \tau_1 c_s^2\ |\mathbf{A}|^{-\frac{5}{3}}, \qquad \theta_2 = \rho z_2 \tau_2\, c_h^2, \qquad z_1 = \frac{\rho_0}{\rho}, \qquad z_2 = \frac{\rho_0 T_0}{\rho\, T} \tag{19}$$

with ρ_0 and T_0 being some reference density and temperature. A formal asymptotic analysis of the system (11a)–(12) was done in [30] and showed that in the stiff relaxation limit when $\tau_1, \tau_2 \to 0$ the stress tensor σ_{ik} and the heat flux h_k tend to

$$\sigma_{ik} = -\frac{1}{6}\rho_0 c_s^2 \tau_1 \left(\partial_k v_i + \partial_i v_k - \frac{2}{3}\left(\partial_m v_m\right)\delta_{ik}\right), \qquad h_k = -\rho_0 T_0 c_h^2 \tau_2 \partial_k T. \tag{20}$$

In other words, in the stiff relaxation limit, the classical Navier-Stokes-Fourier equations are obtained as a special case of the GPR model, with associated shear viscosity $\mu = \frac{1}{6}\rho_0 c_s^2 \tau_1$ and heat conductivity $\kappa = \rho_0 T_0 c_h^2 \tau_2$.

2.4 Turbulent Shallow Water (TSW) Flows

The third and last model considered in this paper is the first-order hyperbolic model for TSW flows. It was introduced by Gavrilyuk et al. in [41] and was also recently studied in [11, 24, 52, 57]. In the following we use the reformulation [16] of the model in terms of a new variable $\mathbf{Q}$, so that the Reynolds stress tensor $\mathbf{P}$ is decomposed as $\mathbf{P} = \mathbf{Q}\mathbf{Q}^{\mathrm{T}}$.

With $P_{ik} = Q_{im}Q_{km}$ and $\partial_m = \frac{\partial}{\partial x_m}$, the hyperbolic model of turbulent shallow water flows with vanishing viscosity regularization reads

$$\partial_t h + \partial_m(h v_m) - \left(\epsilon \frac{\partial h}{\partial x_m}\right) = 0, \tag{21a}$$

$$\partial_t(h v_i) + \partial_k\left(h v_i v_k + \frac{1}{2} g h^2 \delta_{ik} + h P_{ik}\right) - \frac{\partial}{\partial x_m}\left(\epsilon \frac{\partial h v_i}{\partial x_m}\right) = 0, \tag{21b}$$

$$\partial_t Q_{ik} + v_m\,\partial_m\, Q_{ik} + (\partial_m v_i)\ Q_{mk} - \frac{\partial}{\partial x_m}\left(\epsilon \frac{\partial Q_{ik}}{\partial x_m}\right) = \Pi_{ik}, \tag{21c}$$

$$\partial_t \mathcal{E} + \partial_i\left((\mathcal{E}_1 + \mathcal{E}_2)v_i + \left(\frac{1}{2} g h^2 \delta_{ik} + h P_{ik}\right) v_k\right) - \frac{\partial}{\partial x_m}\left(\epsilon \frac{\partial \mathcal{E}}{\partial x_m}\right) = 0. \tag{21d}$$

Here, h denotes the water depth, v_i is the velocity field, and the Reynolds stress tensor in terms of the field Q_{ik} reads $\mathbf{P} = \mathbf{Q}^{\mathrm{T}}\mathbf{Q}$. The total energy $\mathcal{E} = hE = \mathcal{E}_1 + \mathcal{E}_2 + \mathcal{E}_3$ can be decomposed into three contributions with $\mathcal{E}_1 = hE_1 = \frac{1}{2}gh^2$, $\mathcal{E}_2 = hE_2 = \frac{1}{2}h v_i v_i$, and $\mathcal{E}_3 = hE_3 = \frac{1}{2}h Q_{ik}Q_{ik}$, with the energy contribution $\mathcal{E}_3$ due to turbulence. Compared to the other two models (MHD and GPR), the production term is now the tensor Π_{ik}, needed for the consistency of (21a)–(21c) with total energy conservation (21d),

$$\Pi_{ik} = \epsilon \frac{Q_{ik}}{h\,\mathrm{tr}\mathbf{P}}\,\partial_m q_i\,\partial^2_{q_i q_j}\mathcal{E}\,\partial_m q_j. \tag{22}$$

The state vector reads $\mathbf{q} = q_i = (h, hv_i, Q_{ik})$ and in [16] the Hessian matrix was shown to be positive definite when $Q_{ij}Q_{ij}$ is small w.r.t. gh.

3 Numerical Method

3.1 Inviscid Compatible Finite Volume Scheme in One Space Dimension

To facilitate the reading, we first present the approach in one space dimension. At the moment, we furthermore restrict ourselves to the inviscid part of the PDE system, i.e., without the algebraic relaxation source terms and without the vanishing viscosity and its associated entropy production term, hence assuming $\epsilon = 0$. Accordingly, in one dimension, the homogeneous inviscid subsystem of (1) reads

$$\partial_t \mathbf{q} + \partial_x \mathbf{f}_1(\mathbf{q}) + \mathbf{B}_1(\mathbf{q})\partial_x \mathbf{q} = 0. \tag{23}$$

To ease notation, in this section, we denote $\mathbf{f} = \mathbf{f}_1(\mathbf{q})$, $\mathbf{B} = \mathbf{B}_1(\mathbf{q})$, and $F = F_1(\mathbf{q})$, hence dropping the subscripts in the fluxes and in the non-conservative products. A semi-discrete FV scheme for (23) reads

$$\begin{aligned} \frac{\mathrm{d}}{\mathrm{d}t}\mathbf{q}^\ell &= -\frac{\mathcal{F}^{\ell+\frac{1}{2}} - \mathcal{F}^{\ell-\frac{1}{2}}}{\Delta x} - \frac{\mathcal{D}_-^{\ell+\frac{1}{2}} + \mathcal{D}_+^{\ell-\frac{1}{2}}}{\Delta x} \\ &= -\frac{\left(\mathcal{F}^{\ell+\frac{1}{2}} - \mathbf{f}(\mathbf{q}^\ell)\right) + \left(\mathbf{f}(\mathbf{q}^\ell) - \mathcal{F}^{\ell-\frac{1}{2}}\right)}{\Delta x} - \frac{\mathcal{D}_-^{\ell+\frac{1}{2}} + \mathcal{D}_+^{\ell-\frac{1}{2}}}{\Delta x} \end{aligned} \tag{24}$$

with $\mathcal{F}^{\ell\pm\frac{1}{2}}$ the sought thermodynamically compatible numerical flux and $\mathcal{D}_\mp^{\ell\pm\frac{1}{2}}$ a simple centered discretization of the non-conservative product. In order to obtain thermodynamic compatibility of the semi-discrete scheme (24) with total energy conservation, we compute the dot product of (24) with the discrete main field variables $\mathbf{p}^\ell = \partial_{\mathbf{q}}\mathcal{E}(\mathbf{q}^\ell)$ and obtain

$$\begin{aligned} \mathbf{p}^\ell \cdot \frac{\mathrm{d}}{\mathrm{d}t}\mathbf{q}^\ell = \frac{\mathrm{d}}{\mathrm{d}t}\mathcal{E}^\ell &= -\mathbf{p}^\ell \cdot \frac{\left(\mathcal{F}^{\ell+\frac{1}{2}} - \mathbf{f}^\ell\right) + \left(\mathbf{f}^\ell - \mathcal{F}^{\ell-\frac{1}{2}}\right) + \mathcal{D}_-^{\ell+\frac{1}{2}} + \mathcal{D}_+^{\ell-\frac{1}{2}}}{\Delta x} \\ &= -\frac{D_{\mathcal{E},-}^{\ell+\frac{1}{2}} + D_{\mathcal{E},+}^{\ell-\frac{1}{2}}}{\Delta x} = -\frac{F^{\ell+\frac{1}{2}} - F^{\ell-\frac{1}{2}}}{\Delta x}, \end{aligned} \tag{25}$$

where the right and left total energy fluctuations are defined as

$$D_{\mathcal{E},-}^{\ell+\frac{1}{2}} = \mathbf{p}^\ell \cdot (\mathcal{F}^{\ell+\frac{1}{2}} - \mathbf{f}^\ell) + \mathbf{p}^\ell \cdot \mathcal{D}_-^{\ell+\frac{1}{2}}, \quad D_{\mathcal{E},+}^{\ell-\frac{1}{2}} = \mathbf{p}^\ell \cdot (\mathbf{f}^\ell - \mathcal{F}^{\ell-\frac{1}{2}}) + \mathbf{p}^\ell \cdot \mathcal{D}_+^{\ell-\frac{1}{2}}. \tag{26}$$

The numerical total energy fluxes $F^{\ell\pm\frac{1}{2}}$ in (25) are connected to the total energy fluctuations via the usual relations between fluctuations and numerical fluxes

$$D_{\mathcal{E},-}^{\ell+\frac{1}{2}} = F^{\ell+\frac{1}{2}} - F^\ell, \qquad D_{\mathcal{E},+}^{\ell-\frac{1}{2}} = F^\ell - F^{\ell-\frac{1}{2}} \tag{27}$$

with $F^\ell = F(\mathbf{q}^\ell)$. In order to obtain a conservative discretization of the extra conservation law, the numerical total energy flux $F^{\ell+\frac{1}{2}}$ must be the same seen from element ℓ and $\ell+1$. Hence, the sum of the total energy fluctuations at a cell boundary must be equal to the difference of the total energy fluxes $F^{\ell+1}$ and F^ℓ, see also [3, 15–17]. This condition is

obtained by simply summing both equations in (27) at the same interface. For semi-discrete thermodynamic compatibility, we therefore must have

$$D_{\mathcal{E},-}^{\ell+\frac{1}{2}} + D_{\mathcal{E},+}^{\ell+\frac{1}{2}} = \mathbf{p}^{\ell} \cdot \left(\mathcal{F}^{\ell+\frac{1}{2}} - \mathbf{f}^{\ell} + \mathcal{D}_{-}^{\ell+\frac{1}{2}} \right) + \mathbf{p}^{\ell+1} \cdot \left(\mathbf{f}^{\ell+1} - \mathcal{F}^{\ell+\frac{1}{2}} + \mathcal{D}_{+}^{\ell+\frac{1}{2}} \right) = F^{\ell+1} - F^{\ell}. \tag{28}$$

Based on the seminal ideas of Abgrall [1], the thermodynamically compatible numerical flux $\mathcal{F}^{\ell+\frac{1}{2}}$ is now postulated to have the following Abgrall form:

$$\mathcal{F}^{\ell+\frac{1}{2}} = \widetilde{\mathcal{F}}^{\ell+\frac{1}{2}} - \alpha^{\ell+\frac{1}{2}} \left(\mathbf{p}^{\ell+1} - \mathbf{p}^{\ell} \right) \tag{29}$$

with $\widetilde{\mathcal{F}}^{\ell+\frac{1}{2}}$ a simple central approximation of the numerical flux that does not have to guarantee the discrete thermodynamic compatibility of the scheme (24) with the extra conservation law (2) and which is subsequently corrected at the aid of the scalar $\alpha^{\ell+\frac{1}{2}}$ so that discrete thermodynamic compatibility is achieved. We now impose the compatibility condition (28) on the flux (29), including also the non-conservative products. This yields

$$\begin{aligned} &\mathbf{p}^{\ell} \cdot \left(\widetilde{\mathcal{F}}^{\ell+\frac{1}{2}} - \mathbf{f}^{\ell} + \mathcal{D}_{-}^{\ell+\frac{1}{2}} \right) + \mathbf{p}^{\ell+1} \cdot \left(\mathbf{f}^{\ell+1} - \widetilde{\mathcal{F}}^{\ell+\frac{1}{2}} + \mathcal{D}_{+}^{\ell+\frac{1}{2}} \right) \\ &+\alpha^{\ell+\frac{1}{2}} \left(\mathbf{p}^{\ell+1} - \mathbf{p}^{\ell} \right)^2 = F^{\ell+1} - F^{\ell}, \end{aligned} \tag{30}$$

or, equivalently,

$$\begin{aligned} &-\widetilde{\mathcal{F}}^{\ell+\frac{1}{2}} \cdot \left(\mathbf{p}^{\ell+1} - \mathbf{p}^{\ell} \right) + \mathbf{p}^{\ell+1} \cdot \mathbf{f}^{\ell+1} - \mathbf{p}^{\ell} \cdot \mathbf{f}^{\ell} + \mathbf{p}^{\ell+1} \cdot \mathcal{D}_{+}^{\ell+\frac{1}{2}} + \mathbf{p}^{\ell} \cdot \mathcal{D}_{-}^{\ell+\frac{1}{2}} \\ &+\alpha^{\ell+\frac{1}{2}} \left(\mathbf{p}^{\ell+1} - \mathbf{p}^{\ell} \right)^2 = F^{\ell+1} - F^{\ell}. \end{aligned} \tag{31}$$

Equation (31) allows computing the scalar correction factor $\alpha^{\ell+\frac{1}{2}}$, which is the key ingredient of the thermodynamically compatible Abgrall flux (29), as

$$\begin{aligned} \alpha^{\ell+\frac{1}{2}} = &\frac{F^{\ell+1} - F^{\ell} + \widetilde{\mathcal{F}}^{\ell+\frac{1}{2}} \cdot \left(\mathbf{p}^{\ell+1} - \mathbf{p}^{\ell} \right) - \left(\mathbf{p}^{\ell+1} \cdot \mathbf{f}^{\ell+1} - \mathbf{p}^{\ell} \cdot \mathbf{f}^{\ell} \right)}{\left(\mathbf{p}^{\ell+1} - \mathbf{p}^{\ell} \right)^2} \\ &- \frac{\mathbf{p}^{\ell+1} \cdot \mathcal{D}_{+}^{\ell+\frac{1}{2}} + \mathbf{p}^{\ell} \cdot \mathcal{D}_{-}^{\ell+\frac{1}{2}}}{\left(\mathbf{p}^{\ell+1} - \mathbf{p}^{\ell} \right)^2}. \end{aligned} \tag{32}$$

This definition establishes the semi-discrete thermodynamic compatibility of the finite volume scheme (24) with the discrete extra conservation law (25). For vanishing denominator, i.e., $\left(\mathbf{p}^{\ell+1} - \mathbf{p}^{\ell} \right)^2 = 0$, we simply set $\alpha^{\ell+\frac{1}{2}} = 0$, as in this case the states coincide and no correction is needed. Like in [3], we also employ the central flux as underlying numerical flux $\widetilde{\mathcal{F}}^{\ell+\frac{1}{2}}$, i.e., we choose

$$\widetilde{\mathcal{F}}^{\ell+\frac{1}{2}} = \frac{1}{2} \left(\mathbf{f}^{\ell} + \mathbf{f}^{\ell+1} \right). \tag{33}$$

For the fluctuations we use the simple central approximation

$$\mathcal{D}_{\pm}^{\ell+\frac{1}{2}} = \frac{1}{2} \mathbf{B}(\bar{\mathbf{q}}) \left(\mathbf{q}^{\ell+1} - \mathbf{q}^{\ell} \right) \qquad \text{with} \qquad \bar{\mathbf{q}} = \frac{1}{2} \left(\mathbf{q}^{\ell+1} + \mathbf{q}^{\ell} \right). \tag{34}$$

This choice corresponds to a path-conservative scheme [19, 58] based on the straight line segment path and using the mid-point rule to approximate the path integral numerically. However, we emphasize that the precise choice of the central approximations of $\widetilde{\mathcal{F}}^{\ell+\frac{1}{2}}$ and $\mathcal{D}_{\pm}^{\ell+\frac{1}{2}}$ is rather arbitrary, since thermodynamic compatibility is established via the scalar correction factor $\alpha^{\ell+\frac{1}{2}}$ inside the flux (29) and not via the choice of (33) and (34).

We emphasize that, so far, we have only considered the inviscid system (23). A suitable numerical dissipation that is compatible with the first and second principle of thermodynamics and which mimics the parabolic vanishing viscosity terms and the entropy production term in (1) will be added in the next section, directly for the multidimensional extension of the method, following the ideas introduced in [3, 15–17]. We also highlight that the numerical scheme (24) with the flux (29) and (32) is totally general and does not need any kind of particular Godunov parametrization of the flux $\mathbf{f}_1 = \partial_{\mathbf{p}}(v_1 L)$ in terms of a generating potential L, unlike the HTC finite volume schemes presented previously in [15–17].

3.2 Dissipative Compatible Finite Volume Scheme in Multiple Space Dimensions

The generalization of the previous scheme to the multi-dimensional case is straightforward when making use of edge-based/face-based two-point fluxes in normal direction, see also [3, 17]. The computational domain $\Omega \subset \mathbb{R}^d$ in d space dimensions is paved by a general mesh of orthogonal polygonal/polyhedral control volumes Ω^ℓ. The common edge/face of two neighboring polygons/polyhedra Ω^ℓ and Ω^ν is denoted by $\partial\Omega^{\ell\nu} = \Omega^\ell \cap \Omega^\nu$ and N_ℓ is the set of neighbors of element Ω^ℓ.

The semi-discrete finite volume scheme for the discretization of the general PDE system (1) with extra conservation law (2) reads for each control volume Ω^ℓ as follows:

$$\begin{aligned}\frac{\partial \mathbf{q}^\ell}{\partial t} = &- \sum_{\nu\in N_\ell} \frac{\left|\partial\Omega^{\ell\nu}\right|}{\left|\Omega^\ell\right|}\left(\mathcal{F}^{\ell\nu}\cdot\mathbf{n}^{\ell\nu} + \mathcal{D}\left(\mathbf{q}^\ell,\mathbf{q}^\nu\right)\cdot\mathbf{n}^{\ell\nu}\right)\\ &+ \sum_{\nu\in N_\ell} \frac{\left|\partial\Omega^{\ell\nu}\right|}{\left|\Omega^\ell\right|}\left(\mathcal{G}\left(\mathbf{q}^\ell,\mathbf{q}^\nu\right)\cdot\mathbf{n}^{\ell\nu} + \mathbf{P}\left(\mathbf{q}^\ell,\mathbf{q}^\nu\right)\right) + \mathbf{S}(\mathbf{q}^\ell),\end{aligned} \tag{35}$$

where $\mathbf{n}^{\ell\nu}$ is the unit normal vector pointing from element Ω^ℓ to element Ω^ν and thus $\mathbf{n}^{\nu\ell} = -\mathbf{n}^{\ell\nu}$. The two-point numerical flux in normal direction $\mathcal{F}^{\ell\nu}\cdot\mathbf{n}^{\ell\nu}$, the fluctuations $\mathcal{D}\left(\mathbf{q}^\ell,\mathbf{q}^\nu\right)\cdot\mathbf{n}^{\ell\nu}$, the dissipative terms $\mathcal{G}\left(\mathbf{q}^\ell,\mathbf{q}^\nu\right)\cdot\mathbf{n}^{\ell\nu}$, with the related entropy production terms $\mathbf{P}\left(\mathbf{q}^\ell,\mathbf{q}^\nu\right)$, and the algebraic source terms $\mathbf{S}(\mathbf{q}^\ell)$ must verify the compatibility conditions

$$\begin{aligned}&\mathbf{p}^\ell\cdot\left(\mathcal{F}^{\ell\nu}\cdot\mathbf{n}^{\ell\nu} - \mathbf{f}_k^\ell\, n_k^{\ell\nu}\right) + \mathbf{p}^\nu\cdot\left(\mathbf{f}_k^\nu\, n_k^{\ell\nu} - \mathcal{F}^{\ell\nu}\cdot\mathbf{n}^{\ell\nu}\right)\\ &+\mathbf{p}^\ell\cdot\mathcal{D}\left(\mathbf{q}^\ell,\mathbf{q}^\nu\right)\cdot\mathbf{n}^{\ell\nu} + \mathbf{p}^\nu\cdot\mathcal{D}\left(\mathbf{q}^\nu,\mathbf{q}^\ell\right)\cdot\mathbf{n}^{\nu\ell} = \left(F_k^\nu - F_k^\ell\right) n_k^{\ell\nu},\end{aligned} \tag{36}$$

$$\mathbf{p}^\ell\cdot\mathbf{S}\left(\mathbf{q}^\ell\right) = 0. \tag{37}$$

Since the source term satisfies $\mathbf{p}\cdot\mathbf{S} = 0$, the condition (37) holds trivially pointwise and therefore nothing special needs to be done in order to assure compatibility of the algebraic source terms.

Concerning the construction of a thermodynamically compatible numerical flux, as in the one-dimensional case, we start with a simple central discretization of the numerical flux and

of the non-conservative product, i.e., we choose

$$\tilde{\mathcal{F}}^{\ell\imath} \cdot \mathbf{n}^{\ell\imath} = \frac{1}{2}\left(\mathbf{f}_k^{\ell} + \mathbf{f}_k^{\imath}\right) n_k^{\ell\imath} \tag{38}$$

and

$$\mathcal{D}\left(\mathbf{q}^{\ell}, \mathbf{q}^{\imath}\right) \cdot \mathbf{n}^{\ell\imath} = \frac{1}{2}\mathbf{B}_k(\bar{\mathbf{q}}) n_k^{\ell\imath}\left(\mathbf{q}^{\imath} - \mathbf{q}^{\ell}\right), \quad \bar{\mathbf{q}} = \frac{1}{2}\left(\mathbf{q}^{\imath} + \mathbf{q}^{\ell}\right). \tag{39}$$

This discretization is in general not yet compatible with the extra conservation law (2) and therefore the numerical flux (38) needs to be subsequently corrected in order to achieve thermodynamic compatibility. Imposing condition (36), the resulting thermodynamically compatible Abgrall flux [1, 3] reads

$$\mathcal{F}^{\ell\imath} \cdot \mathbf{n}^{\ell\imath} = \tilde{\mathcal{F}}^{\ell\imath} \cdot \mathbf{n}^{\ell\imath} - \alpha^{\ell\imath}\left(\mathbf{p}^{\imath} - \mathbf{p}^{\ell}\right) \tag{40}$$

with the scalar correction factor

$$\begin{aligned}\alpha^{\ell\imath} = & \frac{\left(F_k^{\imath} - F_k^{\ell}\right) n_k^{\ell\imath} + \left(\tilde{\mathcal{F}}^{\ell\imath} \cdot \mathbf{n}^{\ell\imath}\right) \cdot \left(\mathbf{p}^{\imath} - \mathbf{p}^{\ell}\right) - \left(\mathbf{p}^{\imath} \cdot \mathbf{f}_k^{\imath} - \mathbf{p}^{\ell} \cdot \mathbf{f}_k^{\ell}\right) n_k^{\ell\imath}}{\left(\mathbf{p}^{\imath} - \mathbf{p}^{\ell}\right)^2} \\ & - \frac{\left(\mathbf{p}^{\imath} + \mathbf{p}^{\ell}\right) \cdot \mathcal{D}\left(\mathbf{q}^{\ell}, \mathbf{q}^{\imath}\right) \cdot \mathbf{n}^{\ell\imath}}{\left(\mathbf{p}^{\imath} - \mathbf{p}^{\ell}\right)^2}.\end{aligned} \tag{41}$$

It is easy to check that the Abgrall flux (40) together with (38), (39), and (41) satisfies (36) by construction, since the correction factor $\alpha^{\ell\imath}$ is obtained by imposing condition (36) on the numerical flux (40).

Following [3, 15–17], the viscous part of the numerical flux reads

$$\mathcal{G}\left(\mathbf{q}^{\ell}, \mathbf{q}^{\imath}\right) = \epsilon^{\ell\imath} \frac{\mathbf{q}^{\imath} - \mathbf{q}^{\ell}}{\delta^{\ell\imath}} = \epsilon^{\ell\imath} \frac{\Delta \mathbf{q}^{\ell\imath}}{\delta^{\ell\imath}}, \quad \delta^{\ell\imath} = \left\| \mathbf{x}^{\imath} - \mathbf{x}^{\ell} \right\| \tag{42}$$

with the viscosity coefficient at the interface given, for example, by

$$\epsilon^{\ell\imath} = \frac{1}{2}\delta^{\ell\imath} s_{\max}^{\ell\imath}, \qquad s_{\max}^{\ell\imath} = \max\left(\left|\lambda(\mathbf{q}^{\ell})\right|, \left|\lambda(\mathbf{q}^{\imath})\right|\right) \tag{43}$$

with $s_{\max}^{\ell\imath}$, the maximum signal speed at the interface, see e.g., [3, 15–17]. This choice of $\epsilon^{\ell\imath}$ corresponds to a numerical dissipation of the Rusanov-type which vanishes when the mesh size tends to zero. The numerical dissipation can further be reduced by applying a flux-limiter to (43), see e.g., [3, 15, 17]. One may also simply specify a constant but small viscosity coefficient ϵ.

Alternatively, in this paper, we propose a new type of numerical viscosity that is asymptotically second-order accurate for sufficiently fine meshes and which makes direct use of the scalar correction factor $\alpha^{\ell\imath}$ at the interface. The scalar $\alpha^{\ell\imath}$ can be interpreted as a measure of how well the chain and product rules are satisfied at the discrete level. For smooth solutions, we expect that $\alpha^{\ell\imath}$ decreases linearly with the mesh spacing, while at shock waves, we expect $\alpha^{\ell\imath}$ to remain constant or even to increase with decreasing mesh size. It therefore seems to be a natural indicator that may be used to deploy numerical viscosity selectively in the vicinity of shocks and other discontinuities, similar to the principles of entropy viscosity, [48]. In particular, we choose

$$\epsilon^{\ell\imath} = \overline{\alpha}^{\ell\imath} \frac{1}{2}\delta^{\ell\imath} s_{\max}^{\ell\imath} \tag{44}$$

with

$$\overline{\alpha}^{\ell\mathrm{r}} = \begin{cases} \min\left[1, \max\left(0, \frac{|\alpha^{\ell\mathrm{r}}| - \alpha_{\min}}{\alpha_{\max} - \alpha_{\min}}\right)\right] & \text{if } \alpha_{\max} - \alpha_{\min} > 0, \\ 0 & \text{otherwise,} \end{cases} \tag{45}$$

where $\alpha_{\max}$ is the maximum value of $|\alpha|$ taken over the entire computational domain at the previous time step and $\alpha_{\min}$ is a fixed constant, which in this paper has been chosen as $\alpha_{\min} = 3 \times 10^{-4}$ for all those numerical experiments that are based on the new numerical viscosity given by (44).

For both, the MHD equations (6) and the GPR model (11), the related entropy production term reads

$$\mathbf{P}\left(\mathbf{q}^{\ell}, \mathbf{q}^{\mathrm{r}}\right) = \left(0, \mathbf{0}, \Pi^{\ell\mathrm{r}}, \mathbf{0}, \mathbf{0}\right)^{\mathrm{T}}, \tag{46}$$

where the only non-vanishing contribution is in the PDE for the entropy density and is given by

$$\Pi^{\ell\mathrm{r}} = \frac{1}{2}\epsilon^{\ell\mathrm{r}} \frac{\Delta\mathbf{p}^{\ell\mathrm{r}}}{T^{\ell}} \cdot \frac{\Delta\mathbf{q}^{\ell\mathrm{r}}}{\delta^{\ell\mathrm{r}}} = \frac{1}{2}\epsilon^{\ell\mathrm{r}} \frac{\Delta\mathbf{q}^{\ell\mathrm{r}}}{T^{\ell}} \partial^2_{\mathbf{qq}}\tilde{\mathcal{E}}^{\ell\mathrm{r}} \frac{\Delta\mathbf{q}^{\ell\mathrm{r}}}{\delta^{\ell\mathrm{r}}} \geqslant 0, \quad T^{\ell} = \frac{\left(\rho^{\ell}\right)^{\gamma-1}}{(\gamma-1)\, c_v} \mathrm{e}^{\frac{S^{\ell}}{c_v}} \tag{47}$$

with the jumps $\Delta\mathbf{q}^{\ell\mathrm{r}} = \mathbf{q}^{\mathrm{r}} - \mathbf{q}^{\ell}$ and $\Delta\mathbf{p}^{\ell\mathrm{r}} = \mathbf{p}^{\mathrm{r}} - \mathbf{p}^{\ell}$, the temperature T^{ℓ} given in (47) for the ideal gas equation of state. Instead, for the turbulent shallow water model, the discrete entropy production term is more complex. It consists in a production tensor, $\Pi^{\ell\mathrm{r}}_{ik}$, see (22), which is added to the right-hand side of the evolution equation of the tensor Q_{ik}. In its discrete form, it is given by

$$\Pi^{\ell\mathrm{r}}_{ik} = \frac{1}{2}\epsilon^{\ell\mathrm{r}} Q^{\ell}_{ik} \frac{\Delta\mathbf{p}^{\ell\mathrm{r}}}{h^{\ell}\,\mathrm{tr}(\mathbf{P}^{\ell})} \cdot \frac{\Delta\mathbf{q}^{\ell\mathrm{r}}}{\delta^{\ell\mathrm{r}}} = \frac{1}{2}\epsilon^{\ell\mathrm{r}} Q^{\ell}_{ik} \frac{\Delta\mathbf{q}^{\ell\mathrm{r}}}{h^{\ell}\,\mathrm{tr}(\mathbf{P}^{\ell})} \partial^2_{\mathbf{qq}}\tilde{\mathcal{E}}^{\ell\mathrm{r}} \frac{\Delta\mathbf{q}^{\ell\mathrm{r}}}{\delta^{\ell\mathrm{r}}}. \tag{48}$$

In all cases above, the Roe matrix of the Hessian of the energy potential, which appears in the production term (47), reads

$$\partial^2_{\mathbf{qq}}\tilde{\mathcal{E}}^{\ell\mathrm{r}} = \int_0^1 \partial^2_{\mathbf{qq}}\mathcal{E}\left(\tilde{\boldsymbol{\psi}}(s)\right) \mathrm{d}s =: \left(\partial^2_{\mathbf{pp}}\tilde{L}^{\ell\mathrm{r}}\right)^{-1}. \tag{49}$$

Following [3, 16, 17], the former definition is based on the simple straight line segment path in $\mathbf{q}$ variables

$$\tilde{\boldsymbol{\psi}}(s) = \mathbf{q}^{\ell} + s\left(\mathbf{q}^{\mathrm{r}} - \mathbf{q}^{\ell}\right), \qquad 0 \leqslant s \leqslant 1. \tag{50}$$

By construction, the Roe matrix $\partial^2_{\mathbf{qq}}\tilde{\mathcal{E}}^{\ell\mathrm{r}}$ satisfies the Roe property

$$\partial^2_{\mathbf{qq}}\tilde{\mathcal{E}}^{\ell\mathrm{r}} \cdot \left(\mathbf{q}^{\mathrm{r}} - \mathbf{q}^{\ell}\right) = \left(\mathbf{p}^{\mathrm{r}} - \mathbf{p}^{\ell}\right). \tag{51}$$

This allows us to rewrite jumps in terms of the conservative variables $\mathbf{q}$ into jumps in terms of the main field variables (thermodynamic dual variables) $\mathbf{p}$. Note that for, the numerical scheme presented in this paper, it is actually enough to know that such a Roe matrix exists, in order to show the correct sign of the entropy production, while in the practical computations, it is not needed as the product $\Delta\mathbf{p}^{\ell\mathrm{r}} \cdot \Delta\mathbf{q}^{\ell\mathrm{r}}$ can be evaluated directly instead of calculating $\Delta\mathbf{q}^{\ell\mathrm{r}}\partial^2_{\mathbf{qq}}\tilde{\mathcal{E}}^{\ell\mathrm{r}}\Delta\mathbf{q}^{\ell\mathrm{r}}$, see also (47) and (48).

The discrete form of the algebraic source terms for the GPR model (11) simply reads

$$\mathbf{S}\left(\mathbf{q}^{\ell}\right)=\begin{pmatrix} 0 \\ \mathbf{0} \\ \dfrac{\alpha_{ik}^{\ell}\alpha_{ik}^{\ell}}{\theta_1^{\ell}(\tau_1)T^{\ell}}+\dfrac{\beta_k^{\ell}\beta_k^{\ell}}{\theta_2^{\ell}(\tau_2)T^{\ell}} \\ -\dfrac{\alpha_{ik}^{\ell}}{\theta_1^{\ell}(\tau_1)} \\ -\dfrac{\beta_i^{\ell}}{\theta_2^{\ell}(\tau_2)} \end{pmatrix}=\begin{pmatrix} 0 \\ \mathbf{0} \\ \pi^{\ell} \\ -\dfrac{\alpha_{ik}^{\ell}}{\theta_1^{\ell}(\tau_1)} \\ -\dfrac{\beta_i^{\ell}}{\theta_2^{\ell}(\tau_2)} \end{pmatrix}, \tag{52}$$

while for the MHD equations $\mathbf{S}\left(\mathbf{q}^{\ell}\right)=\mathbf{0}$.

Theorem 1 (Cell entropy inequality) *For the MHD equations* (6) *and for the GPR model* (11)*, the HTC FV scheme* (35) *satisfies the following cell entropy inequality*:

$$\frac{\partial \rho S}{\partial t}+\sum_{\imath\in N_{\ell}}\frac{\left|\Omega^{\ell\imath}\right|}{\left|\Omega^{\ell}\right|}\left(\mathcal{F}_{\rho S}\left(\mathbf{q}^{\ell},\mathbf{q}^{\imath}\right)\cdot\mathbf{n}^{\ell\imath}-\mathcal{G}_{\rho S}\left(\mathbf{q}^{\ell},\mathbf{q}^{\imath}\right)\cdot\mathbf{n}^{\ell\imath}\right)\geqslant 0. \tag{53}$$

Proof Taking the discrete equation for the entropy density from (35), which contains only conservative fluxes, substituting (40) together with (38), (39), (41), and (52), we obtain

$$\begin{aligned}&\frac{\partial\left(\rho S\right)^{\ell}}{\partial t}+\frac{1}{\left|\Omega^{\ell}\right|}\sum_{\imath\in N_{\ell}}\left|\partial\Omega^{\ell\imath}\right|\left(\mathcal{F}_{\rho S}\left(\mathbf{q}^{\ell},\mathbf{q}^{\imath}\right)\cdot\mathbf{n}^{\ell\imath}-\mathcal{G}_{\rho S}\left(\mathbf{q}^{\ell},\mathbf{q}^{\imath}\right)\cdot\mathbf{n}^{\ell\imath}\right)\\&=\frac{1}{\left|\Omega^{\ell}\right|}\sum_{\imath\in N_{\ell}}\left|\partial\Omega^{\ell\imath}\right|\frac{1}{2}\epsilon^{\ell\imath}\frac{\Delta\mathbf{q}^{\ell\imath}}{T^{\ell}}\cdot\partial^2_{\mathbf{qq}}\tilde{\mathcal{E}}^{\ell\imath}\frac{\Delta\mathbf{q}^{\ell\imath}}{\delta^{\ell\imath}}+\pi^{\ell}\geqslant 0,\end{aligned}$$

where the positivity of the right-hand side is obtained, thanks to $\pi^{\ell}\geqslant 0$ and due to the positive semi-definiteness of the Hessian $\partial^2_{\mathbf{qq}}\mathcal{E}$. Note that in the MHD equations, there are no algebraic relaxation sources, hence $\pi^{\ell}=0$.

Theorem 2 (Nonlinear stability in the energy norm) *The finite volume scheme* (35) *with the Abgrall flux* (40) *together with* (38), (39), (41) *in combination with the viscous flux, the source terms and the discrete entropy production terms defined in* (42), (47)*, and (52) is nonlinearly stable in the energy norm in the sense that, for vanishing boundary fluxes, we have*

$$\int_{\Omega}\frac{\partial\mathcal{E}}{\partial t}\mathrm{d}\mathbf{x}=0. \tag{54}$$

Proof To prove nonlinear stability in the energy norm, we first derive a semi-discrete total energy conservation law. For this purpose, we take the dot product of the discrete main field variables $\mathbf{p}^{\ell}$ with the semi-discrete scheme (35):

$$\begin{aligned}\mathbf{p}^{\ell}\cdot\frac{\partial\mathbf{q}^{\ell}}{\partial t}=&-\frac{1}{\left|\Omega^{\ell}\right|}\sum_{\imath\in N_{\ell}}\left|\partial\Omega^{\ell\imath}\right|\left(\mathbf{p}^{\ell}\cdot\left(\mathcal{F}^{\ell\imath}\cdot\mathbf{n}^{\ell\imath}\right)+\mathbf{p}^{\ell}\cdot\left(\mathcal{D}\left(\mathbf{q}^{\ell},\mathbf{q}^{\imath}\right)\cdot\mathbf{n}^{\ell\imath}\right)\right)\\&+\frac{1}{\left|\Omega^{\ell}\right|}\sum_{\imath\in N_{\ell}}\left|\partial\Omega^{\ell\imath}\right|\left(\mathbf{p}^{\ell}\cdot\left(\mathcal{G}\left(\mathbf{q}^{\ell},\mathbf{q}^{\imath}\right)\cdot\mathbf{n}^{\ell\imath}\right)+\mathbf{p}^{\ell}\cdot\mathbf{P}\left(\mathbf{q}^{\ell},\mathbf{q}^{\imath}\right)\right)+\mathbf{p}^{\ell}\cdot\mathbf{S}(\mathbf{q}^{\ell}).\end{aligned}$$

Due to (37), the contribution of the algebraic source terms in the former equation cancels. Moreover, adding and subtracting the terms corresponding to $\frac{1}{2}\mathbf{p}^{\iota}\cdot\mathcal{D}\left(\mathbf{q}^{\iota},\mathbf{q}^{\ell}\right)\cdot\mathbf{n}^{\iota\ell}$, $\frac{1}{2}\mathbf{p}^{\iota}\cdot\mathcal{F}^{\ell\iota}$, and $\frac{1}{2}\mathbf{p}^{\iota}\cdot\mathcal{G}\left(\mathbf{q}^{\ell},\mathbf{q}^{\iota}\right)\cdot\mathbf{n}^{\ell\iota}$, we get

$$
\begin{aligned}
\frac{\partial\mathcal{E}^{\ell}}{\partial t} = &-\frac{1}{\left|\Omega^{\ell}\right|}\sum_{\iota\in N_{\ell}}\left|\partial\Omega^{\ell\iota}\right|\left(\frac{1}{2}\left(\mathbf{p}^{\ell}+\mathbf{p}^{\iota}\right)\cdot\mathcal{F}^{\ell\iota}\cdot\mathbf{n}^{\ell\iota}\right)\\
&-\frac{1}{\left|\Omega^{\ell}\right|}\sum_{\iota\in N_{\ell}}\left|\partial\Omega^{\ell\iota}\right|\left(\frac{1}{2}\left(\mathbf{p}^{\ell}-\mathbf{p}^{\iota}\right)\cdot\mathcal{F}^{\ell\iota}\cdot\mathbf{n}^{\ell\iota}\right)\\
&-\frac{1}{\left|\Omega^{\ell}\right|}\sum_{\iota\in N_{\ell}}\left|\partial\Omega^{\ell\iota}\right|\left(\frac{1}{2}\mathbf{p}^{\ell}\cdot\mathcal{D}\left(\mathbf{q}^{\ell},\mathbf{q}^{\iota}\right)\cdot\mathbf{n}^{\ell\iota}+\frac{1}{2}\mathbf{p}^{\iota}\cdot\mathcal{D}\left(\mathbf{q}^{\iota},\mathbf{q}^{\ell}\right)\cdot\mathbf{n}^{\iota\ell}\right)\\
&-\frac{1}{\left|\Omega^{\ell}\right|}\sum_{\iota\in N_{\ell}}\left|\partial\Omega^{\ell\iota}\right|\left(\frac{1}{2}\mathbf{p}^{\ell}\cdot\mathcal{D}\left(\mathbf{q}^{\ell},\mathbf{q}^{\iota}\right)\cdot\mathbf{n}^{\ell\iota}-\frac{1}{2}\mathbf{p}^{\iota}\cdot\mathcal{D}\left(\mathbf{q}^{\iota},\mathbf{q}^{\ell}\right)\cdot\mathbf{n}^{\iota\ell}\right)\\
&+\frac{1}{\left|\Omega^{\ell}\right|}\sum_{\iota\in N_{\ell}}\left|\partial\Omega^{\ell\iota}\right|\left(\frac{1}{2}\left(\mathbf{p}^{\ell}+\mathbf{p}^{\iota}\right)\cdot\mathcal{G}\left(\mathbf{q}^{\ell},\mathbf{q}^{\iota}\right)\cdot\mathbf{n}^{\ell\iota}\right)\\
&+\frac{1}{\left|\Omega^{\ell}\right|}\sum_{\iota\in N_{\ell}}\left|\partial\Omega^{\ell\iota}\right|\left(\frac{1}{2}\left(\mathbf{p}^{\ell}-\mathbf{p}^{\iota}\right)\cdot\mathcal{G}\left(\mathbf{q}^{\ell},\mathbf{q}^{\iota}\right)\cdot\mathbf{n}^{\ell\iota}+\mathbf{p}^{\ell}\cdot\mathbf{P}\left(\mathbf{q}^{\ell},\mathbf{q}^{\iota}\right)\right).
\end{aligned}
$$

The compatibility condition (36) together with $\mathbf{n}^{\iota\ell}=-\mathbf{n}^{\ell\iota}$ leads to

$$
\begin{aligned}
\frac{\partial\mathcal{E}^{\ell}}{\partial t} = &-\frac{1}{\left|\Omega^{\ell}\right|}\sum_{\iota\in N_{\ell}}\left|\partial\Omega^{\ell\iota}\right|\frac{1}{2}\left(F_{k}^{\iota}-F_{k}^{\ell}\right)n_{k}^{\ell\iota}\\
&-\frac{1}{2\left|\Omega^{\ell}\right|}\sum_{\iota\in N_{\ell}}\left|\partial\Omega^{\ell\iota}\right|\left(\mathbf{p}^{\ell}\cdot\mathbf{f}_{k}^{\ell}-\mathbf{p}^{\iota}\cdot\mathbf{f}_{k}^{\iota}\right)n_{k}^{\ell\iota}\\
&-\frac{1}{2\left|\Omega^{\ell}\right|}\sum_{\iota\in N_{\ell}}\left|\partial\Omega^{\ell\iota}\right|\left(\mathbf{p}^{\ell}+\mathbf{p}^{\iota}\right)\cdot\mathcal{F}^{\ell\iota}\cdot\mathbf{n}^{\ell\iota}\\
&-\frac{1}{2\left|\Omega^{\ell}\right|}\sum_{\iota\in N_{\ell}}\left|\partial\Omega^{\ell\iota}\right|\left(\mathbf{p}^{\ell}\cdot\mathcal{D}\left(\mathbf{q}^{\ell},\mathbf{q}^{\iota}\right)+\mathbf{p}^{\iota}\cdot\mathcal{D}\left(\mathbf{q}^{\iota},\mathbf{q}^{\ell}\right)\right)\cdot\mathbf{n}^{\ell\iota}\\
&+\frac{1}{\left|\Omega^{\ell}\right|}\sum_{\iota\in N_{\ell}}\left|\partial\Omega^{\ell\iota}\right|\left(\frac{1}{2}\left(\mathbf{p}^{\ell}+\mathbf{p}^{\iota}\right)\cdot\mathcal{G}\left(\mathbf{q}^{\ell},\mathbf{q}^{\iota}\right)\cdot\mathbf{n}^{\ell\iota}\right)\\
&+\frac{1}{\left|\Omega^{\ell}\right|}\sum_{\iota\in N_{\ell}}\left|\partial\Omega^{\ell\iota}\right|\left(\frac{1}{2}\left(\mathbf{p}^{\ell}-\mathbf{p}^{\iota}\right)\cdot\mathcal{G}\left(\mathbf{q}^{\ell},\mathbf{q}^{\iota}\right)\cdot\mathbf{n}^{\ell\iota}+\mathbf{p}^{\ell}\cdot\mathbf{P}\left(\mathbf{q}^{\ell},\mathbf{q}^{\iota}\right)\right).
\end{aligned}
$$

Since the integral of the normal vector over a closed surface vanishes, the following identity holds:

$$
\sum_{\iota\in N_{\ell}}\left|\partial\Omega^{\ell\iota}\right|\mathbf{n}^{\ell\iota}=0. \tag{55}
$$

Adding $\mathbf{p}^\ell \cdot \mathbf{f}_k^\ell + F_k^\ell$ multiplied by (55) and using (42) and (47), we get

$$\begin{aligned}
\frac{\partial \mathcal{E}^\ell}{\partial t} = & -\frac{1}{|\Omega^\ell|} \sum_{\iota \in N_\ell} \left|\partial\Omega^{\ell\iota}\right| \frac{1}{2} \left(F_k^\iota + F_k^\ell\right) n_k^{\ell\iota} \\
& + \frac{1}{2|\Omega^\ell|} \sum_{\iota \in N_\ell} \left|\partial\Omega^{\ell\iota}\right| \left(\mathbf{p}^\iota \cdot \mathbf{f}_k^\iota + \mathbf{p}^\ell \cdot \mathbf{f}_k^\ell\right) n_k^{\ell\iota} - \frac{1}{2|\Omega^\ell|} \sum_{\iota \in N_\ell} \left|\partial\Omega^{\ell\iota}\right| \left(\mathbf{p}^\ell + \mathbf{p}^\iota\right) \cdot \mathcal{F}^{\ell\iota} \cdot \mathbf{n}^{\ell\iota} \\
& - \frac{1}{2|\Omega^\ell|} \sum_{\iota \in N_\ell} \left|\partial\Omega^{\ell\iota}\right| \left(\mathbf{p}^\ell \cdot \mathcal{D}\left(\mathbf{q}^\ell, \mathbf{q}^\iota\right) + \mathbf{p}^\iota \cdot \mathcal{D}\left(\mathbf{q}^\iota, \mathbf{q}^\ell\right)\right) \cdot \mathbf{n}^{\ell\iota} \\
& + \frac{1}{|\Omega^\ell|} \sum_{\iota \in N_\ell} \left|\partial\Omega^{\ell\iota}\right| \left(\frac{1}{2}\left(\mathbf{p}^\ell + \mathbf{p}^\iota\right) \cdot \mathcal{G}\left(\mathbf{q}^\ell, \mathbf{q}^\iota\right) \cdot \mathbf{n}^{\ell\iota}\right) \\
& + \frac{1}{|\Omega^\ell|} \sum_{\iota \in N_\ell} \left|\partial\Omega^{\ell\iota}\right| \left(\frac{1}{2}\left(\mathbf{p}^\ell - \mathbf{p}^\iota\right) \cdot \epsilon^{\ell\iota} \frac{\Delta \mathbf{q}^{\ell\iota}}{\delta^{\ell\iota}} + \frac{1}{2} \epsilon^{\ell\iota} \Delta \mathbf{q}^{\ell\iota} \cdot \partial^2_{\mathbf{qq}} \tilde{\mathcal{E}}^{\ell\iota} \frac{\Delta \mathbf{q}^{\ell\iota}}{\delta^{\ell\iota}}\right).
\end{aligned}$$

The last two terms cancel, thanks to the Roe property (51) that must be satisfied by the Hessian of the total energy density. Hence, we obtain the following discrete form of the total energy conservation law:

$$\begin{aligned}
\frac{\partial \mathcal{E}^\ell}{\partial t} = & -\frac{1}{|\Omega^\ell|} \sum_{\iota \in N_\ell} \left|\partial\Omega^{\ell\iota}\right| F_k^{\ell\iota} n_k^{\ell\iota} = -\frac{1}{|\Omega^\ell|} \sum_{\iota \in N_\ell} \left|\partial\Omega^{\ell\iota}\right| \frac{1}{2} \left(F_k^\iota + F_k^\ell\right) n_k^{\ell\iota} \\
& - \frac{1}{|\Omega^\ell|} \sum_{\iota \in N_\ell} \left|\partial\Omega^{\ell\iota}\right| \frac{1}{2} \left(\mathbf{p}^\iota \cdot (\mathcal{F}^{\ell\iota} \cdot \mathbf{n}^{\ell\iota} - \mathbf{f}_k^\iota n_k^{\ell\iota}) + \mathbf{p}^\ell \cdot (\mathcal{F}^{\ell\iota} \cdot \mathbf{n}^{\ell\iota} - \mathbf{f}_k^\ell n_k^{\ell\iota})\right) \\
& + \frac{1}{|\Omega^\ell|} \sum_{\iota \in N_\ell} \left|\partial\Omega^{\ell\iota}\right| \frac{1}{2} \left(\mathbf{p}^\ell + \mathbf{p}^\iota\right) \cdot \left(\mathcal{G}\left(\mathbf{q}^\ell, \mathbf{q}^\iota\right) \cdot \mathbf{n}^{\ell\iota}\right) \\
& - \frac{1}{2|\Omega^\ell|} \sum_{\iota \in N_\ell} \left|\partial\Omega^{\ell\iota}\right| \left(\mathbf{p}^\ell \cdot \mathcal{D}\left(\mathbf{q}^\ell, \mathbf{q}^\iota\right) + \mathbf{p}^\iota \cdot \mathcal{D}\left(\mathbf{q}^\iota, \mathbf{q}^\ell\right)\right) \cdot \mathbf{n}^{\ell\iota}.
\end{aligned}$$

The sought nonlinear stability in the energy norm is then easily obtained as

$$\int_\Omega \frac{\partial \mathcal{E}}{\partial t} \mathrm{d}\mathbf{x} = \sum_\ell \left|\Omega^\ell\right| \frac{\partial \mathcal{E}^\ell}{\partial t} = 0,$$

where we have assumed the fluxes and fluctuations to be zero at the boundary and we have made use of the telescopic sum property since the sum of the numerical total energy fluxes $F_k^{\ell\iota} n_k^{\ell\iota}$ at the internal interfaces cancels.

4 Numerical Results

To assess the proposed HTC-FV schemes, we analyse several benchmarks for the different models studied, namely the MHD equations, the GPR model for continuum mechanics and the hyperbolic model for turbulent shallow water flows.

Table 1 L^2-error norms and convergence rates for the smooth MHD vortex problem obtained with the semi-discrete HTC finite volume scheme at time $t = 0.25$ without any numerical viscosity, $\epsilon = 0$. $N_x = N_y$ denotes the number of control volumes of the mesh in each direction

N_x	$\|\rho\|^2$	$\|\rho v_1\|^2$	$\|\rho S\|^2$	$\|B_1\|^2$	$\mathcal{O}(\rho)$	$\mathcal{O}(\rho v_1)$	$\mathcal{O}(\rho S)$	$\mathcal{O}(B_1)$
64	2.31E−03	1.85E−03	2.31E−03	2.41E−03				
128	5.80E−04	4.69E−04	5.78E−04	6.08E−04	2.0	2.0	2.0	2.0
256	1.45E−04	1.18E−04	1.45E−04	1.52E−04	2.0	2.0	2.0	2.0
512	3.63E−05	2.95E−05	3.61E−05	3.81E−05	2.0	2.0	2.0	2.0
1 024	9.08E−06	7.37E−06	9.03E−06	9.53E−06	2.0	2.0	2.0	2.0

In all test cases, the fourth-order Runge-Kutta method is employed for time integration and the time step is computed attending to the CFL-type condition

$$\Delta t = \frac{\mathrm{CFL}}{\frac{|\lambda^x_{\max}|}{\Delta x} + \frac{|\lambda^y_{\max}|}{\Delta y} + 2\epsilon\left(\frac{1}{\Delta x^2} + \frac{1}{\Delta y^2}\right)}, \tag{56}$$

where Δx, Δy are the characteristic mesh spacing in x and y directions and $|\lambda^x_{\max}|$, $|\lambda^y_{\max}|$ refer to the corresponding maximum absolute eigenvalues. Unless stated, the contrary the artificial viscosity, ϵ, is set to zero.

4.1 MHD Equations

4.1.1 Numerical Convergence Study

To assess the accuracy of the proposed method, a smooth MHD vortex test case is analysed, [5, 15]. More precisely, we consider the computational domain $\Omega = [0, 10]^2$ and an exact solution of the form

$$v_1 = \mathrm{e}^{\frac{1}{2}(1-r^2)}(5-y), \quad v_2 = \mathrm{e}^{\frac{1}{2}(1-r^2)}(x-5), \quad v_3 = 0, \quad p = \frac{1}{2}\mathrm{e} - \frac{1}{2}r^2\mathrm{e}^{-(r^2-1)},$$
$$\rho = 1, \quad B_1 = \mathrm{e}^{\frac{1}{2}(1-r^2)}(5-y), \quad B_2 = \mathrm{e}^{\frac{1}{2}(1-r^2)}(x-5), \quad B_3 = 0$$

with $r^2 = (x-5)^2 + (y-5)^2$. The model parameters are set to $\gamma = \frac{5}{3}$, $\epsilon = 0$ and periodic boundary conditions are defined for all boundaries. The L^2 -errors at time $t = 0.25$ obtained for a set of successively refined meshes, with $N_x \in \{32, 64, 128, 256, 512\}$ divisions along each axis, are reported in Table 1. The expected second order of convergence is reached. We now repeat the same test, but with the new numerical viscosity $\epsilon^{\ell\iota}$ given by (44). The obtained numerical convergence rates are shown in Table 2, confirming that for sufficiently fine meshes ($N_x \geqslant 256$), the method asymptotically reaches second order of accuracy and the errors become identical to the results in Table 1, with $\epsilon = 0$, as expected.

4.1.2 Riemann Problems

The behaviour of the scheme in the presence of strong waves including shocks is studied through a set of Riemann problems described in [15]. The constant left and right states at the initial time are given in Table 3; $\gamma = \frac{5}{3}$ is employed in all tests. The initial discontinuity is positioned at $x_c = 0$ for RP1 and RP4 and at $x_c = -0.1$ for RP2 and RP3 while the

Table 2 L^2-error norms and convergence rates for the smooth MHD vortex problem obtained with the semi-discrete HTC finite volume scheme at time $t = 0.25$ with the new numerical viscosity given by (44). $N_x = N_y$ denotes the number of control volumes of the mesh in each direction

N_x	$\|\rho\|^2$	$\|\rho v_1\|^2$	$\|\rho S\|^2$	$\|B_1\|^2$	$\mathcal{O}(\rho)$	$\mathcal{O}(\rho v_1)$	$\mathcal{O}(\rho S)$	$\mathcal{O}(B_1)$
64	1.09E−02	1.68E−01	8.45E−02	1.68E−01				
128	1.03E−02	9.67E−02	4.89E−02	9.66E−02	0.1	0.8	0.8	0.8
256	1.45E−04	1.18E−04	1.45E−04	1.52E−04	6.1	9.7	8.4	9.3
512	3.63E−05	2.95E−05	3.61E−05	3.81E−05	2.0	2.0	2.0	2.0
1 024	9.08E−06	7.37E−06	9.03E−06	9.53E−06	2.0	2.0	2.0	2.0

Table 3 Initial left and right states for density ρ, velocity $\mathbf{v} = (v_1, v_2, v_3)$, pressure p, and magnetic field $\mathbf{B} = (B_x, B_y, B_z)$ for the Riemann problems of the ideal MHD equations

Case	ρ	v_1	v_2	v_3	p	B_x	B_y	B_z
RP1 L	1.0	0.0	0.0	0.0	1.0	$\frac{3}{4}$	1.0	0.0
R	0.125	0.0	0.0	0.0	0.1	$\frac{3}{4}$	−1.0	0.0
RP2 L	1.08	1.2	0.01	0.5	0.95	$\frac{2.0}{\sqrt{4\pi}}$	$\frac{3.6}{\sqrt{4\pi}}$	$\frac{2.0}{\sqrt{4\pi}}$
R	0.989 1	−0.013 1	0.026 9	0.010 037	0.971 59	$\frac{2.0}{\sqrt{4\pi}}$	$\frac{4.024\,4}{\sqrt{4\pi}}$	$\frac{2.002\,6}{\sqrt{4\pi}}$
RP3 L	1.7	0.0	0.0	0.0	1.7	1.1	1.0	0.0
R	0.2	0.0	0.0	−1.496 89	0.2	1.1	$\frac{2.785\,9}{\sqrt{4\pi}}$	$\frac{2.192\,1}{\sqrt{4\pi}}$
RP4 L	1.0	0.0	0.0	0.0	1.0	1.3	1.0	0.0
R	0.4	0.0	0.0	0.0	0.4	1.3	−1.0	0.0

computational domain, $\Omega = [-0.5, 0.5]$, is discretized using a uniform mesh of 1 000 control volumes. For this test problem, the numerical viscosity is chosen according to (43) with flux limiter [17]. In Fig. 1, a good agreement is observed between the obtained numerical solution and the reference solution computed with the exact Riemann solver for MHD equations kindly provided by Falle and Komissarov [31, 32].

4.1.3 MHD Orszag-Tang Vortex

The third test analysed is the classical Orszag-Tang vortex benchmark. We consider the setup provided in [15, 53] which consists on a computational domain $\Omega = [0, 2\pi]^2$ with periodic boundary conditions, the initial fields given by

$$\rho = \gamma^2, \quad p = \gamma = \frac{5}{3}, \quad v_1 = -\sin(y), \quad v_2 = \sin(x), \quad v_3 = 0,$$
$$B_1 = -\sin(y), \quad B_2 = \sin(2x), \quad B_3 = 0,$$

and the new numerical viscosity is set according to (44). The numerical solution at times $t \in \{0.5, 2.0, 3.0, 5.0\}$ obtained with the new HTC-FV scheme on a mesh made of $2\,048 \times 2\,048$ cells is shown in Fig. 2. A good qualitative agreement can be observed with numerical solutions available in the bibliography, see e.g., [6, 7, 15]. In Fig. 3, we report the contour plots of $\overline{\alpha}$, according to (45). We observe how the numerical viscosity is activated only in the vicinity of shocks, discontinuities or steep gradients.

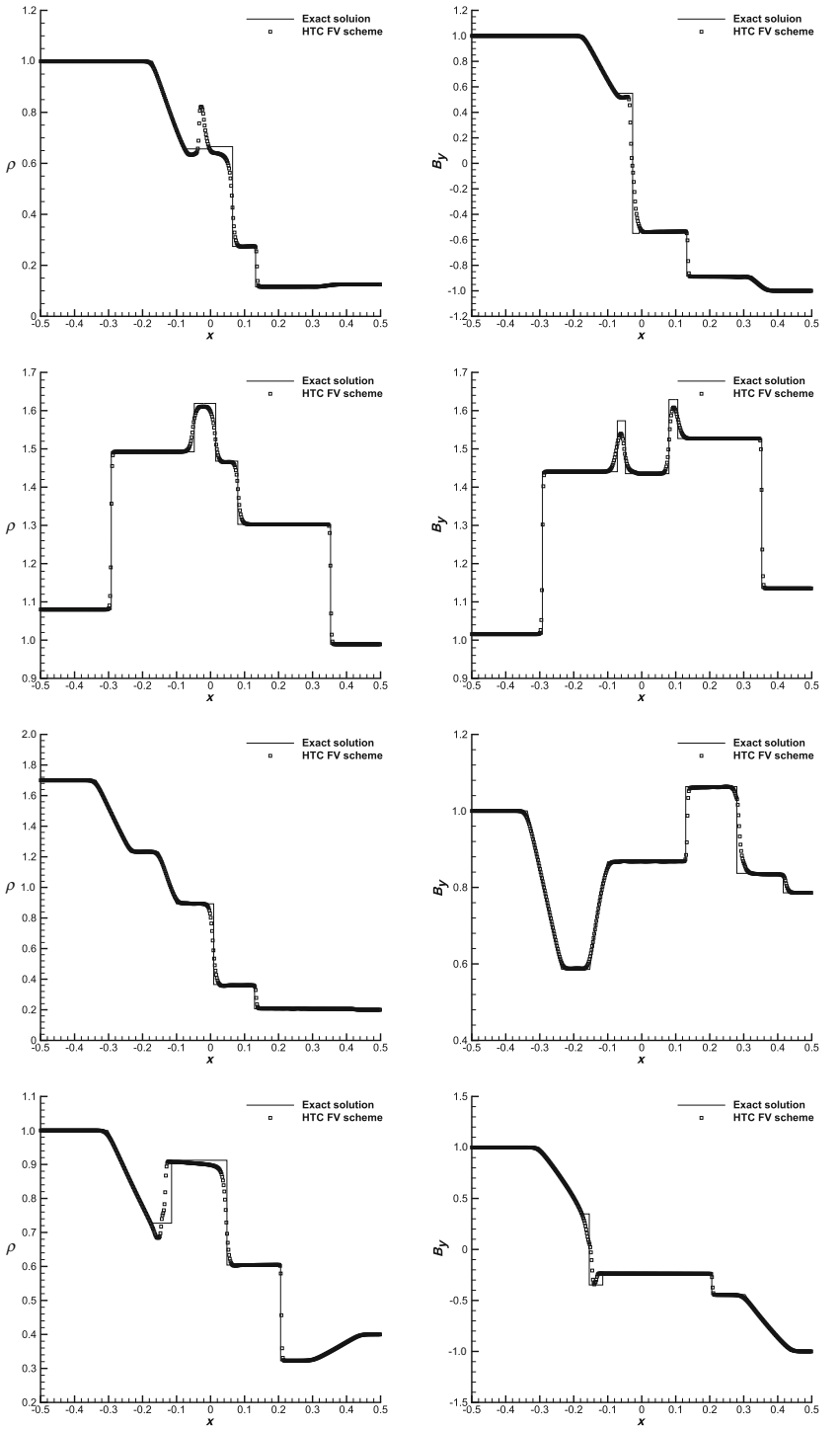

Fig. 1 Exact and numerical solutions for MHD Riemann problems RP1–RP4 (from top to bottom). Density (left) and magnetic field component B_y (right) at $t = 0.1$, $t = 0.2$, $t = 0.15$, and $t = 0.16$

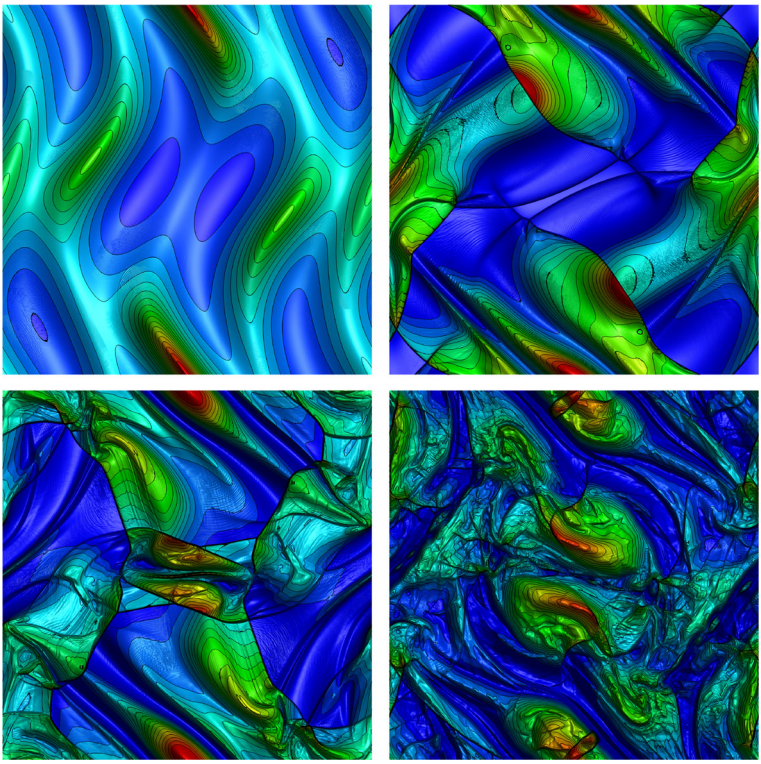

Fig. 2 Density contours obtained with the new semi-discrete HTC-FV scheme for the inviscid Orszag-Tang vortex system at times $t \in \{0.5, 2, 3, 5\}$ (from top left to bottom right)

4.1.4 MHD Rotor Problem

As fourth test, we study the MHD rotor problem initially proposed in [8]. Accordingly, the pressure and the magnetic field are assumed to be initially constant with $p = 1$ and $\mathbf{B} = (2.5/\sqrt{4\pi}, 0, 0)^{\mathrm{T}}$ while the density and velocity are set to $\rho = 10$ and $\mathbf{v} = \boldsymbol{\omega} \times \mathbf{x}$ if $0 \leqslant \|\mathbf{x}\| \leqslant 0.1$ and to $\rho = 1$ and $\mathbf{v} = (0, 0, 0)$ otherwise. To complete the test setup, we define $\gamma = 1.4$, we compute ϵ using the new numerical viscosity (44) and we discretize the computational domain, $\Omega = [-0.5, 0.5]^2$, using a Cartesian grid of 1 024 $\times$ 1 024 cells. The mass density, hydrodynamic pressure, Mach number and magnetic pressure obtained, at time $t = 0.25$, using the new general HTC-FV scheme are reported in Fig. 4. Again a good qualitative agreement is observed with reference numerical data in the literature, [6–8, 15]. To illustrate the behavior of the new numerical viscosity, we also include in Fig. 5-left the value of $\overline{\alpha}$ which shows that the viscosity is deployed locally at shocks and discontinuities.

4.1.5 MHD Blast Wave Problem

The last test studied for the MHD system, the blast wave problem, [8], is well known to be very challenging for numerical methods mainly due to the presence of large pressure jumps on the initial condition,

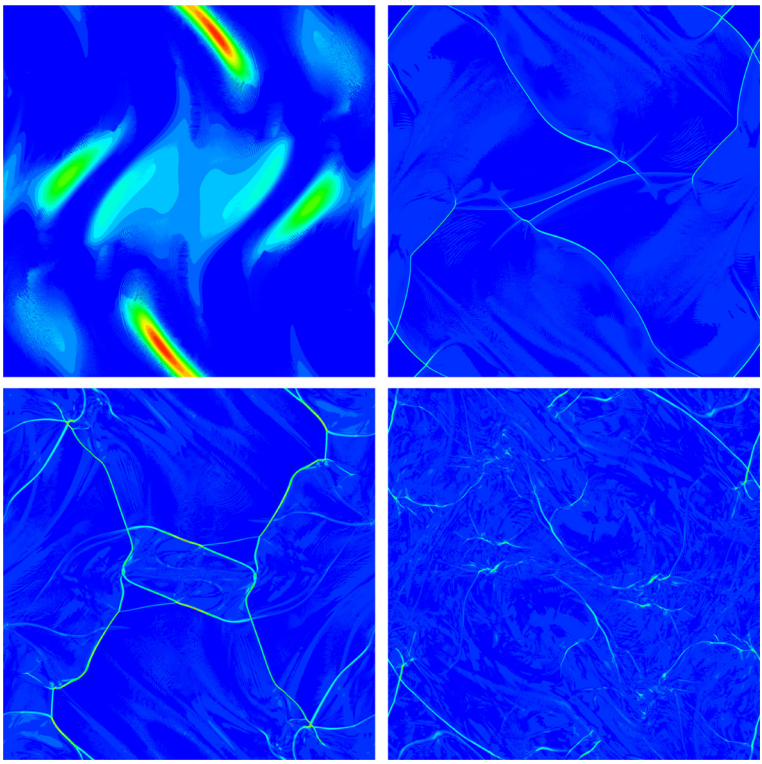

Fig. 3 Equidistant contour plots of $\overline{\alpha} \in [0, 1]$ obtained with the new semi-discrete HTC-FV scheme for the inviscid Orszag-Tang vortex system at times $t \in \{0.5, 2, 3, 5\}$ (from top left to bottom right)

$$\rho = 1, \qquad \mathbf{v} = (0, 0, 0), \qquad p = \begin{cases} 1\ 000 & \text{if } \|\mathbf{x}\| < 0.1, \\ 0.1 & \text{otherwise,} \end{cases} \qquad \mathbf{B} = (100/\sqrt{4\pi}, 0, 0),$$

which is defined in the computational domain $\Omega = [-0.6, 0.6]^2$. We run a simulation on a Cartesian grid made of $1\ 024 \times 1\ 024$ cells setting $\gamma = 1.4$ and choosing the new numerical viscosity according to (44). The obtained density, hydrostatic pressure, velocity magnitude and magnetic pressure fields are shown in Fig. 6 for $t = 0.01$. They agree qualitatively well with numerical solutions available in the literature, e.g., see [7, 8, 15]. As for the rotor test case, the value of $\overline{\alpha}$ is also reported at the final time in the right panel of Fig. 5. We observe that the viscosity is deployed locally at shocks and discontinuities.

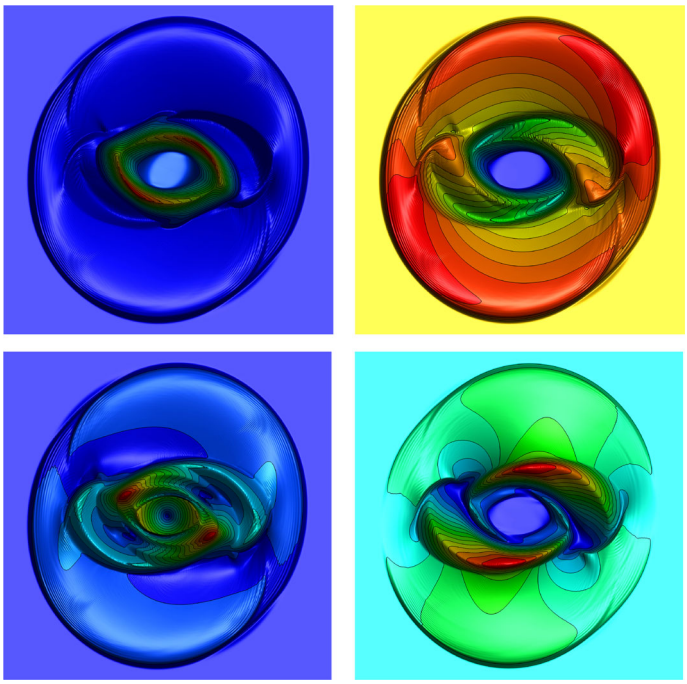

Fig. 4 Contour plots of the mass density (top left), the hydrodynamic pressure (top right), the Mach number (bottom left), and the magnetic pressure (bottom right) obtained with the new HTC-FV scheme for the MHD rotor problem at time $t = 0.25$

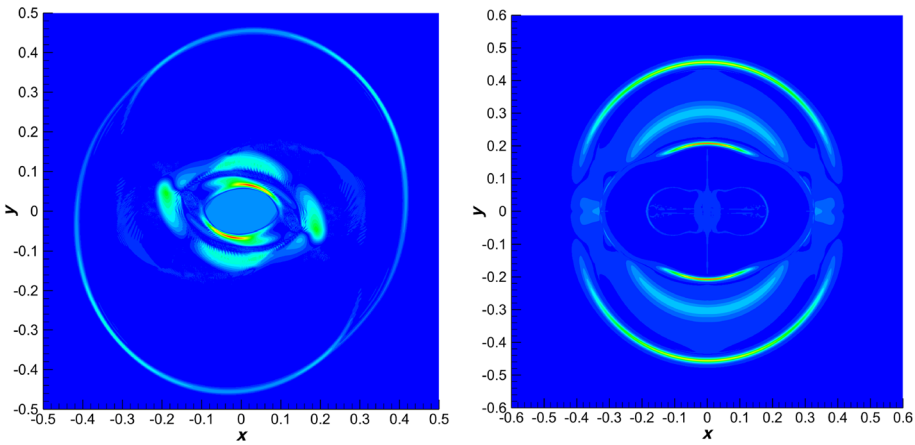

Fig. 5 Contour plots of $\overline{\alpha}$ obtained with the new HTC-FV scheme using the new viscosity in (44) for the MHD rotor problem at time $t = 0.25$ (left) and for the two-dimensional MHD blast wave problem at time $t = 0.01$ (right)

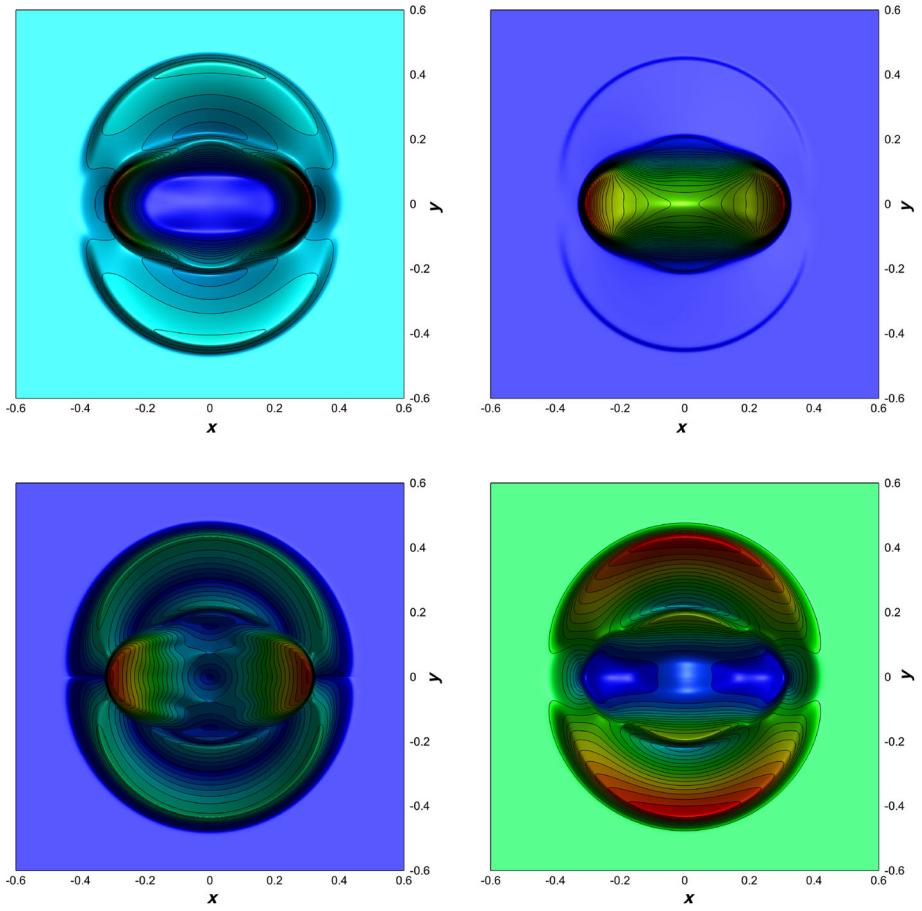

Fig. 6 Contour plots of the mass density (top left), the hydrodynamic pressure (top right), the velocity magnitude (bottom left), and the magnetic pressure (bottom right) obtained with the new HTC-FV scheme for the two-dimensional MHD blast wave problem at time $t = 0.01$

4.2 GPR Model of Continuum Mechanics

4.2.1 Numerical Convergence Study

The isentropic vortex benchmark [51] is employed to assess the accuracy of the HTC-FV scheme for the Euler subsystem embedded in the GPR model. We consider the computational domain $\Omega = [0, 10]^2$ and define the initial condition following the exact steady solution of the Euler equations

Table 4 L^2-error norms and convergence rates for the isentropic vortex problem obtained with the semi-discrete HTC-FV scheme at time $t = 0.25$. N denotes the number of mesh divisions on each axis direction

N	$\|\rho\|^2$	$\|\rho v_1\|^2$	$\|\rho v_2\|^2$	$\|\rho S\|^2$	$\mathcal{O}(\rho)$	$\mathcal{O}(\rho v_1)$	$\mathcal{O}(\rho v_2)$	$\mathcal{O}(\rho S)$
32	7.25E−03	9.32E−03	9.32E−03	1.11E−03				
64	1.84E−03	2.43E−03	2.43E−03	3.14E−04	2.0	1.9	1.9	1.8
128	4.60E−04	6.14E−04	6.14E−04	8.02E−05	2.0	2.0	2.0	2.0
256	1.15E−04	1.54E−04	1.54E−04	2.01E−05	2.0	2.0	2.0	2.0
512	2.88E−05	3.85E−05	3.85E−05	5.04E−06	2.0	2.0	2.0	2.0

$$\begin{cases} \rho = 1 + (1 + \delta T)^{\frac{1}{\gamma - 1}}, \begin{pmatrix} v_1 \\ v_2 \end{pmatrix} = \frac{\varepsilon}{2\pi} \mathrm{e}^{\frac{1-r^2}{2}} \begin{pmatrix} 5 - y \\ x - 5 \end{pmatrix}, \\ p = 1 + (1 + \delta T)^{\frac{\gamma}{\gamma - 1}}, \ \delta T = -\frac{(\gamma - 1)\varepsilon^2}{8\gamma\pi^2} \mathrm{e}^{1-r^2} \end{cases} \tag{57}$$

with $r^2 = (x - 5)^2 + (y - 5)^2$ and $\varepsilon = 5$ the vortex strength. Moreover, we set $c_s = 0$, $c_h = 0$, $\gamma = 1.4$. The L^2-errors and convergence rates obtained, at time $t = 0.25$, for a set of successively refined grids are reported in Table 4. We can observe that the sought second order of accuracy is reached for the density, linear momentum components, and the entropy density.

4.2.2 Shear Motion

The shear motion benchmark is used to assess the behaviour of the method in both the solid and fluid limits of the GPR model. We define the computational domain $\Omega = [-0.5, 0.5]$ and the initial conditions: $\rho = 1$, $v_1 = v_3 = 0$, $v_2 = -0.1$ for $x < 0$ and $v_2 = 0.1$ for $x \geqslant 0$, $p = 1$, $\mathbf{A} = \mathbf{I}$, and $\mathbf{J} = \mathbf{0}$. Moreover, we set $c_s = c_h = 1$, $\gamma = 1.4$, and $\epsilon = 10^{-6}$. Four simulations are run, the solid limit, $\tau_1 = \tau_2 = 10^{20}$, and three viscous fluids, $\tau_1 \ll 1$, with viscosities $\mu = \kappa = 10^{-2}$, $\mu = \kappa = 10^{-3}$, and $\mu = \kappa = 10^{-4}$. The final simulation time is $t = 0.4$ and the domain is discretized using 6 144 control volumes. The numerical results obtained with the new HTC-FV scheme are depicted in Fig. 7. The reference solution in the fluid limit is given by the exact solution of the first problem of Stokes for the incompressible Navier-Stokes equations, see [18, 30], and reads

$$v_2(x, t) = 0.1 \operatorname{erf}\left(\frac{1}{2} \frac{x}{\sqrt{\frac{\mu}{\rho} t}} \right).$$

Meanwhile, the reference solution in the solid limit has been computed solving (11) on a very fine mesh of 10 000 cells using a classical second order accurate MUSCL-Hancock type TVD finite volume scheme, [75]. An excellent agreement between numerical and reference solutions can be observed in all cases.

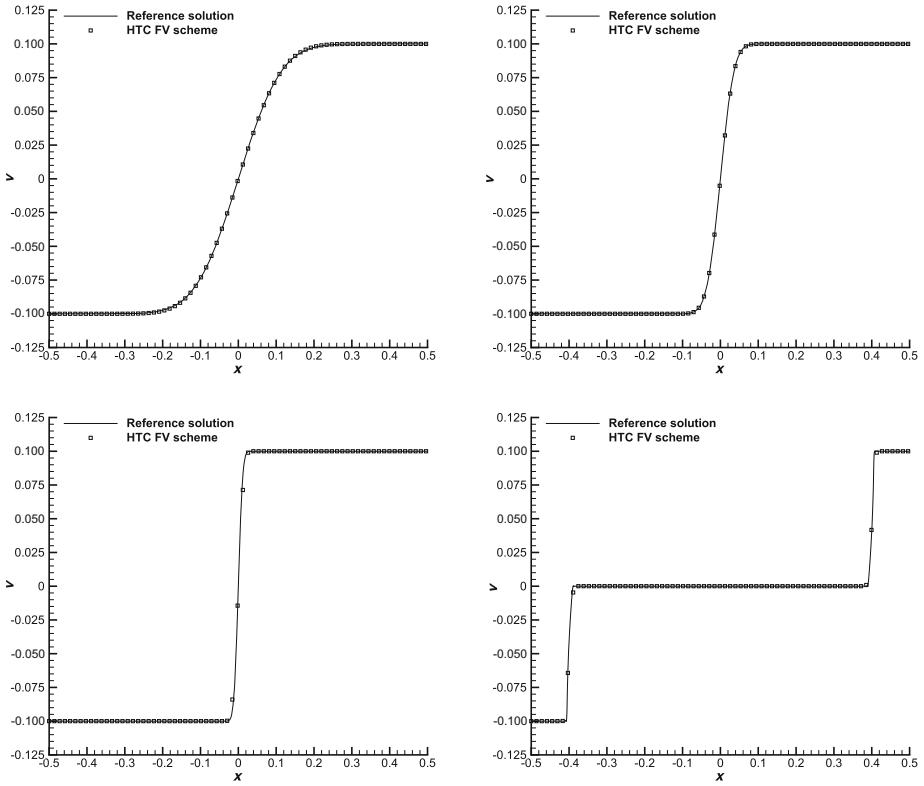

Fig. 7 Second component of the velocity obtained with the new HTC finite volume scheme for a simple one-dimensional shear motion in viscous fluids, $\mu = 10^{-2}$ (top left), $\mu = 10^{-3}$ (top right), $\mu = 10^{-4}$ (bottom left), and for an ideal elastic solid (bottom right). The continuous black line reports the exact solution for each viscous fluid and the reference solution for the solid limit obtained using a TVD FV scheme on 1 000 cells

4.2.3 Riemann Problems

We now study six different Riemann problems, four for the Euler equations (RP1, RP2, RP3, RP4) and two for the complete GPR model (RP5, RP6), [17, 75]. The initial states at the two sides of the initial discontinuity point, x_c, are detailed in Table 5. The numerical solutions obtained with the novel HTC-FV scheme using the numerical viscosity (43) with flux limiter [17] are reported in Figs. 8, 9, 10, and 11 together with the corresponding reference solutions. As in [17] the exact Riemann solver for the Euler equations [75] has been employed to compute the reference solution for RP1–4. Meanwhile, to obtain those of RP5–6, the GPR model has been solved using a classical second order TVD finite volume scheme of the MUSCL-Hancock type on a very fine mesh of 128 000 elements. In this scheme, instead of the entropy inequality, the total energy conservation law is discretized. An excellent agreement is observed for all test cases.

4.2.4 Viscous Shock

To further assess the behaviour of the new HTC FV scheme in the fluid limit, we analyse a steady viscous shock of Mach number $Ma = 2$ and $Pr = 0.75$ which has a known exact

Table 5 Left and right states for the initial condition of the six Riemann problems considered and location of the initial discontinuity (x_c)

RP	ρ_L	u_L	v_L	p_L	ρ_R	u_R	v_R	p_R	x_c
RP1	1.0	0.0	0.0	1.0	0.125	0.0	0.0	0.1	0.0
RP2	5.999 24	19.597 5	0.0	460.894	5.992 42	−6.196 33	0.0	46.095	−0.2
RP3	1.0	−2.0	0.0	0.4	1.0	+2.0	0.0	0.4	0.0
RP4	1.0	−1.0	0.0	1.0	1.0	+1.0	0.0	1.0	0.0
RP5	1.0	0.0	−0.2	1.0	0.5	0.0	+0.2	0.5	0.0
RP6	1.0	0.0	−0.2	1.0	0.5	0.0	+0.2	0.5	0.0

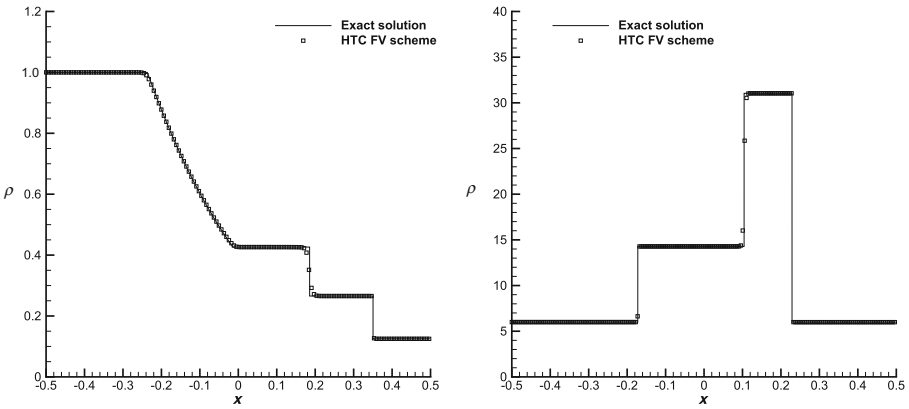

Fig. 8 Density field of the Sod problem (left) and RP2 (right) obtained at times $t = 0.2$ and $t = 0.035$ using the new HTC FV scheme on meshes made of 1 536 and 6 144 cells, respectively. The black solid line corresponds to the exact solution taken from [75]

solution for the Navier-Stokes equations [9, 12, 30]. We define the computational domain $\Omega = [-0.5, 0.5]$ and place the initial shock wave at $x = 0$. Moreover, the states in front of the shock are $\rho_0 = 1$, $v_1^0 = 2$, $v_2^0 = v_3 = 0$, and $p^0 = 1/\gamma$ so the sound speed is $c^0 = 1$ and the initial data for the distortion field and for the thermal impulse are $\mathbf{A} = \sqrt[3]{\rho}\,\mathbf{I}$ and $\mathbf{J} = \mathbf{0}$. Taking the remaining parameters of the GPR model as $c_v = 2.5$, $c_h = c_s = 10$, $\mu = 2 \times 10^{-2}$, and $\lambda = \left(9 + \frac{1}{3}\right) 5 \times 10^{-2}$, then the shock Reynolds number is $Re_s = \rho^0 c^0 M_s L \mu^{-1} = 100$, where we have considered the reference length $L = 1$. The simulation with the new HTC-FV scheme proposed in this paper is run until time $t = 0.25$ on a grid of 1 024 cells. In Fig. 12, we observe an excellent agreement between the numerical results and the reference Navier-Stokes solution.

4.2.5 Solid Rotor

The solid rotor test case [17] is a classical benchmark for the GPR model in the solid limit. The initial condition, defined in $\Omega = [-1, 1]^2$, reads

$$\rho = 1, \quad (v_1, v_2, v_3) = \begin{cases} \left(\frac{-y}{R}, \frac{x}{R}, 0\right) & \text{if } \|\mathbf{x}\| \leqslant R, \\ \mathbf{0} & \text{otherwise,} \end{cases} \quad p = 1, \quad \mathbf{A} = \mathbf{I}, \quad \mathbf{J} = \mathbf{0}.$$

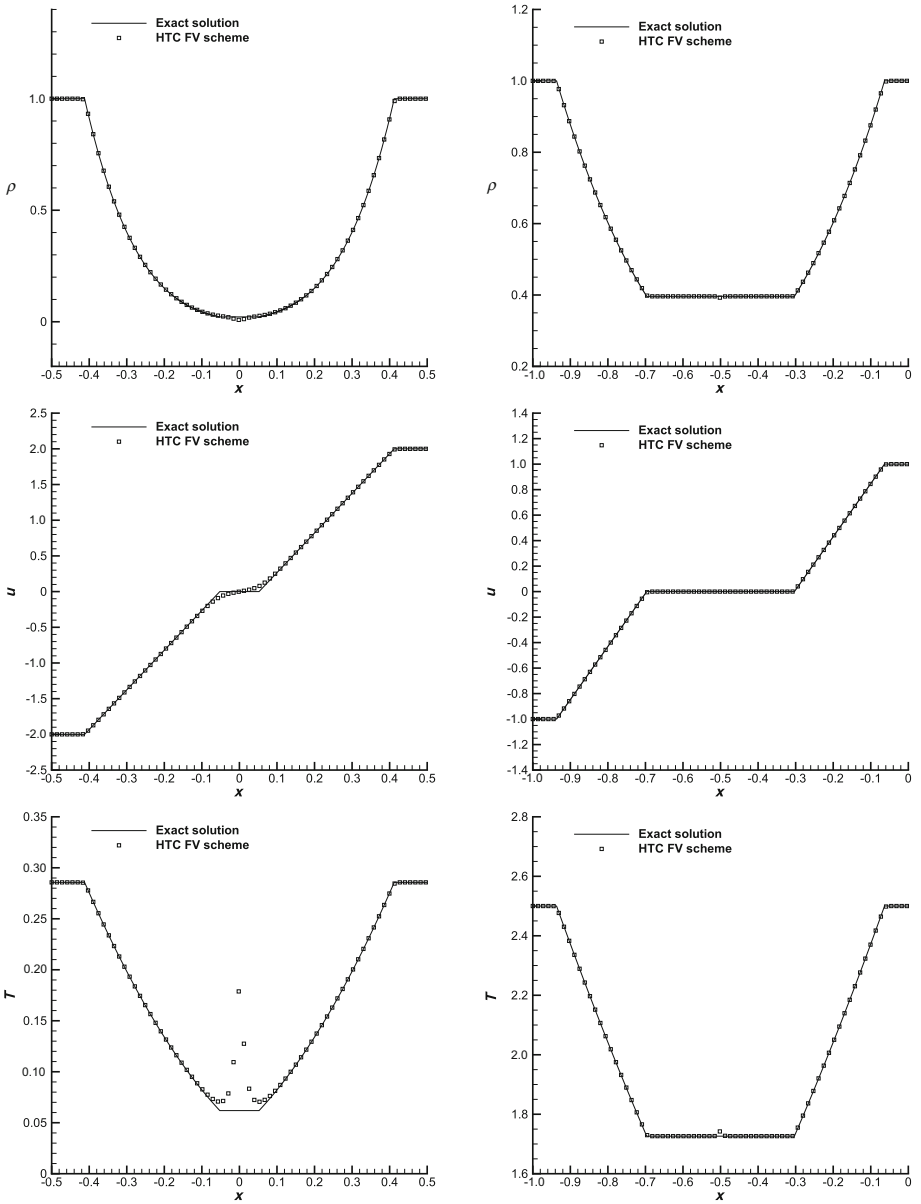

Fig. 9 Results for the double rarefaction Riemann problems. Left: classical 123 problem at $t = 0.15$. Right: modified double rarefaction test at $t = 0.15$. The solution obtained using the new HTC FV scheme on a grid composed of 6 144 cells is represented using squares while the exact solution, see [75], is depicted using a solid line

Since we are in the solid case, we set $\tau_1 = \tau_2 = 10^{20}$ while the shear sound speed and the parameter related to the finite speed heat wave propagation are fixed to $c_s = 1.0$ and $c_h = 1.0$. Finally, we assume transmissive boundary conditions everywhere. The contour plot

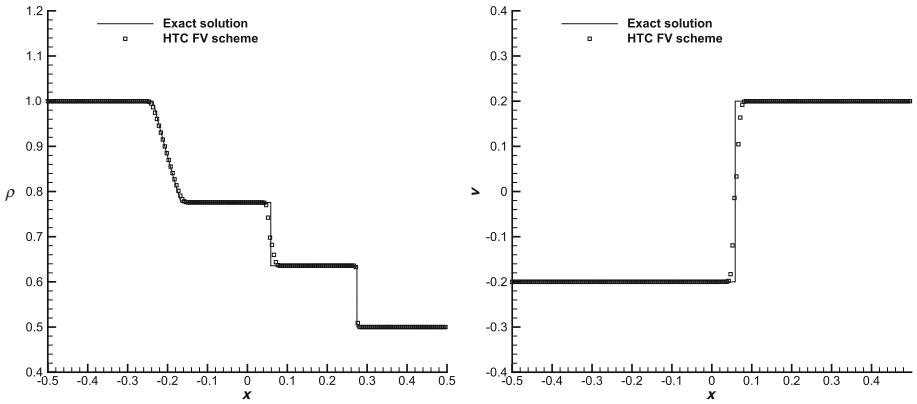

Fig. 10 Desity and velocity obtained for RP5 at $t = 0.2$ by solving the GPR model in the stiff relaxation limit ($\mu = \kappa = 5 \times 10^{-5}$). The black solid line corresponds to the known exact solution for the compressible Euler equations, see [75]

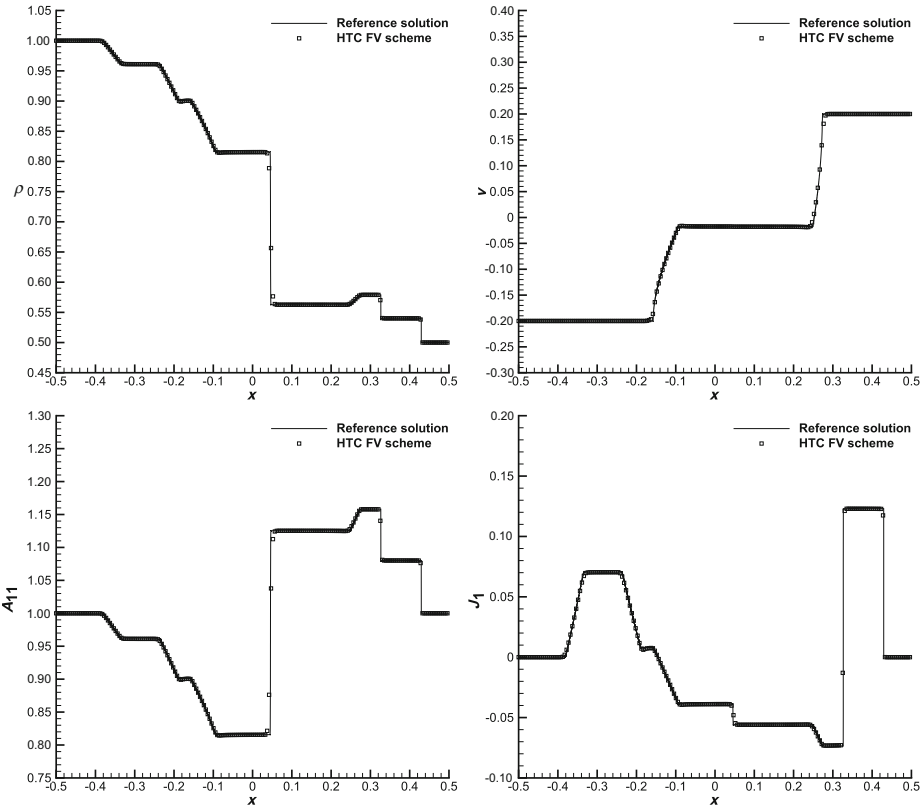

Fig. 11 Density, velocity v_2, distortion field component A_{11} and heat flux J_1 of RP6 at $t = 0.2$ computed solving the GPR model in the solid limit, $\tau_1 = \tau_2 = 10^{20}$, using the new HTC FV scheme on a grid made of 6 144 control volumes. A second-order MUSCL-Hancock scheme has been used to obtain the reference solution on a mesh of 128 000 cells

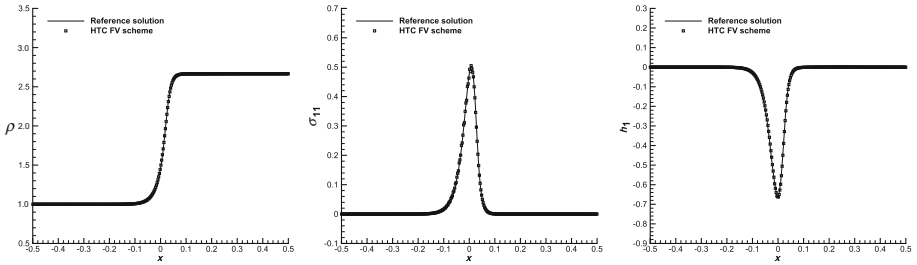

Fig. 12 Density ρ, stress σ_{11}, and heat flux h_1 obtained for the viscous shock test case using the new HTC FV scheme

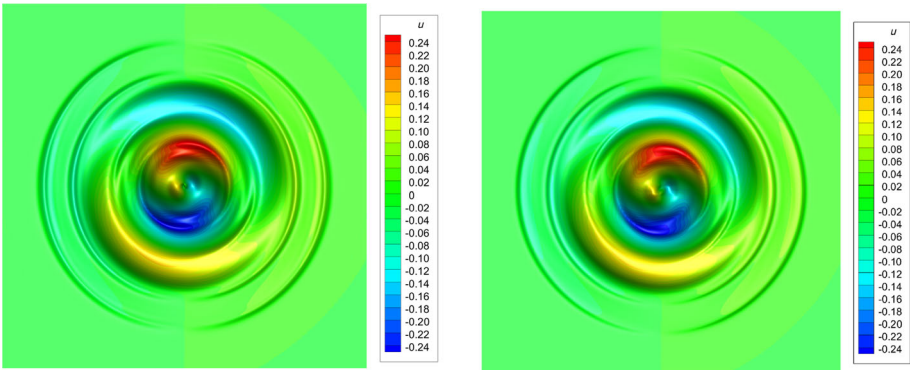

Fig. 13 Contour plots of v_1 for the solid rotor problem obtained using the new HTC FV scheme (left) and reference solution obtained using MUSCL (right)

of v_1 obtained at time $t = 0.3$ on a mesh of 261 121 Cartesian cells is depicted in Fig. 13. The solution obtained using a classical second order MUSCL-Hancock scheme is also depicted for comparison. We observe a very good agreement, also with the results published previously in [17].

4.2.6 Lid-Driven Cavity

The lid-driven cavity is a classical test for incompressible flows with a well-known reference solution [42] and thus may be the optimal candidate to validate the incompressible fluid limit of the GPR solver in the low Mach number regime, [3, 17, 18, 30]. We define the computational domain $\Omega = [0, 1]^2$ with no-slip walls, $\mathbf{v} = \mathbf{0}$, in the lateral and bottom boundaries and a unitary horizontal lid velocity on the upper boundary, $\mathbf{v} = (1, 0, 0)$. Initially the fluid is considered to be at rest, i.e., $\mathbf{v} = \mathbf{0}$, $\mathbf{A} = \mathbf{I}$, and $\mathbf{J} = \mathbf{0}$ with $\rho = 1$ and $p = 100$. Furthermore, the model parameters are set to $\mu = 10^{-2}$, $c_s = 8$, $c_h = 2$, and $\tau_2 = 10^{-2}$, so the associated Reynolds and Mach numbers are $Re = 100$, $Ma = 0.08$. Figure 14 reports the numerical solution obtained at $t = 10$ using the novel HTC-FV scheme on a grid of 65 025 cells and with artificial viscosity $\epsilon = 10^{-3}$. Moreover, a one-dimensional cut fo the velocity components

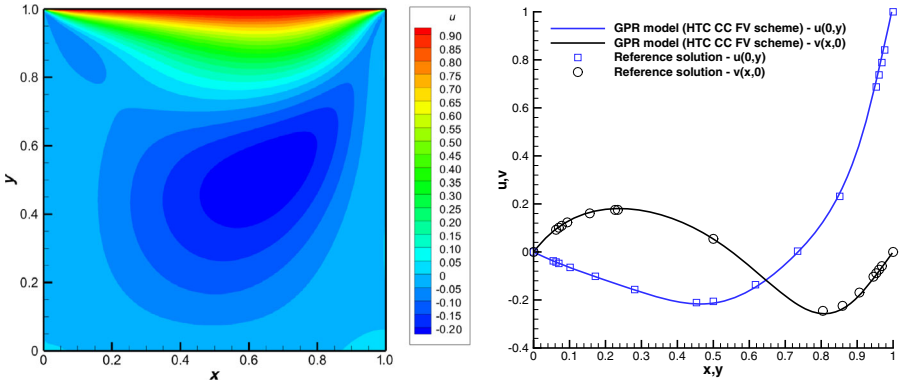

Fig. 14 Lid-driven cavity at Reynolds number $Re = 100$. Results at time $t = 10$ using the new HTC FV scheme applied to the GPR model. Contours of v_1 (left) and comparison of the velocity with the reference solution [42] on one-dimensional cuts along the x and y axes (right)

along the mean axis of the domain is depicted together with the reference solution in [42]. An almost perfect match is observed.

4.2.7 Double Shear Layer

We now apply the HTC-FV scheme for the GPR model to the shear-layer benchmark proposed in [10] and widely extended to assess compressible flow solvers [3, 17, 18, 30, 73]. The computational domain is $\Omega = [0, 1]^2$, we define periodic boundary conditions everywhere and the initial condition is defined as

$$v_1 = \begin{cases} \tanh(\tilde{\rho}(y - 0.25)) & \text{if } y \leqslant 0.5, \\ \tanh(\tilde{\rho}(0.75 - y)) & \text{if } y > 0.5, \end{cases} \quad v_2 = \delta \sin(2\pi x), \quad v_3 = 0,$$

$$\rho = 1, \quad p = \frac{10^2}{\gamma}, \quad \mathbf{A} = \mathbf{I}, \quad \mathbf{J} = \mathbf{0}, \quad \delta = 0.05, \quad \tilde{\rho} = 30.$$

The remaining model parameters are set to $\mu = 2 \times 10^{-3}$, $c_v = 1$, $c_s = 8$, $c_h = 2$, and $\tau_2 = 4 \times 10^{-3}$, leading to a characteristic Mach number of $Ma = 10^{-1}$. A simulation is run using the new HTC-FV scheme on a grid made of 4 000 × 4 000 cells up to $t = 1.8$. The obtained distortion field component A_{12} is plotted in Fig. 15 at times $t \in \{0.4, 0.8, 1.2, 1.8\}$. See [10, 17, 18, 30, 73] for a qualitative comparison of the obtained results with diverse numerical schemes and for a more detailed analysis of the flow evolution.

4.3 Turbulent Shallow Water (TSW) Flows

4.3.1 Riemann Problems

We now study the behaviour of the proposed HTC-FV method in the framework of the turbulent shallow water model (21). To this end, we consider the three Riemann problems already proposed in [16] whose non-zero initial left and right states and final times are recalled in Table 6. The computational domain $\Omega = [0, 1]$ is discretized at the aid of 56 000 control volumes for RP1 and 28 000 cells for RP2 and RP3. All simulations are run with the numerical viscosity given by (43) with flux limiter [16]. In Figs. 16–18, we report the solution obtained

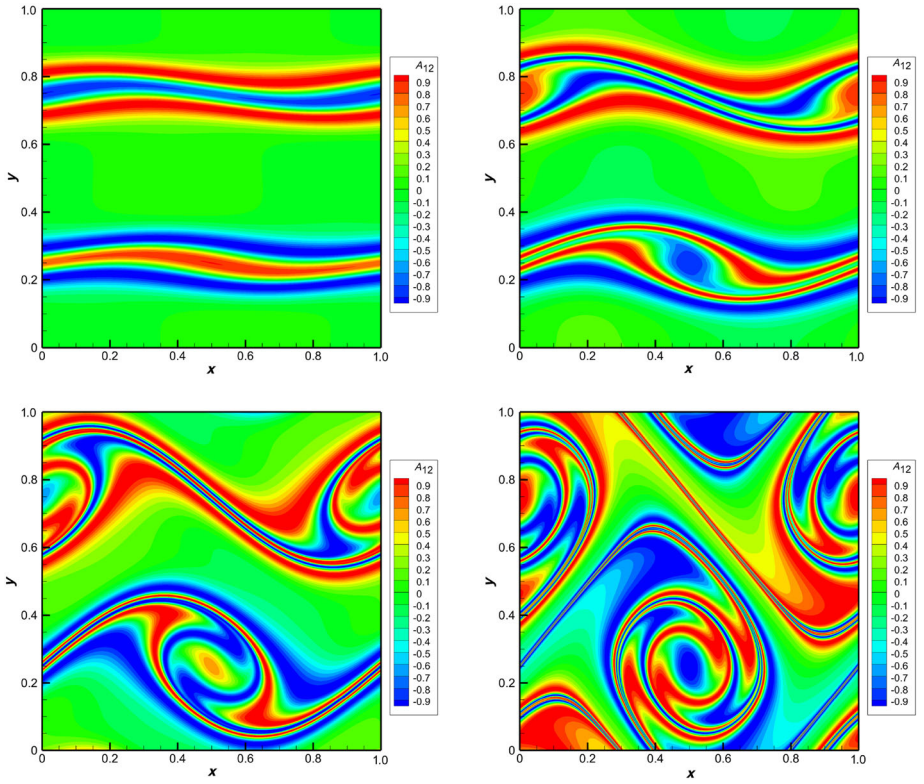

Fig. 15 Double shear layer test case: numerical results obtained with the new thermodynamically compatible cell-centered HTC finite volume scheme presented in this paper and applied to the GPR model of continuum mechanics setting $\mu = 2 \times 10^{-3}$. Distortion field component A_{12} at times $t = 0.4$ (top left), $t = 0.8$ (top right), $t = 1.2$ (bottom left), and $t = 1.8$ (bottom right)

Table 6 Initial left and right states for the Riemann problems RP1–RP3 for the TSW model

Test	h^{L}	h^{R}	v_2^{L}	v_2^{R}	Q_{11}^{L}	Q_{11}^{R}	Q_{12}^{L}	Q_{12}^{R}	$Q_{22}^{\mathrm{L,R}}$	t
RP1	0.02	0.01	0	0	0.01	0.01	0	0	10^{-4}	0.5
RP2	0.01	0.01	+0.01	−0.01	0.02	0.02	0	0	0.02	10
RP3	0.01	0.01	0	0	0.1	0.1	0.2	0.1	0.1	0.75

using the new HTC-FV scheme for (21), the split scheme proposed in [52] and the results from a direct numerical simulation (DNS) of the vanishing viscosity limit of the equations on a sufficiently fine mesh [16]. An excellent agreement is observed between the three schemes even for the complex wave pattern of RP3, where the discrete thermodynamic compatibility of the non-conservative hyperbolic equations has shown to be essential to properly capture all waves.

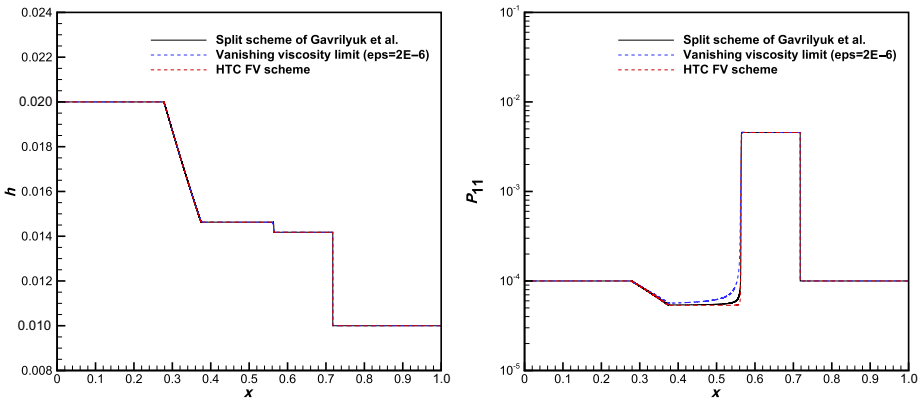

Fig. 16 Turbulent shallow water flow: comparison of the numerical solutions obtained with different methods for Riemann problem RP1 at time $t = 0.5$: split scheme of [41] using 250 000 elements (solid black line); fourth-order ADER-DG scheme ($N = 3$) on 11 200 elements [16] applied to the vanishing viscosity limit of system (21a)–(21d) with viscosity coefficient $\epsilon = 2 \times 10^{-6}$ (dashed blue line); the new thermodynamically compatible HTC FV scheme presented in this paper using 56 000 elements (dashed red line)

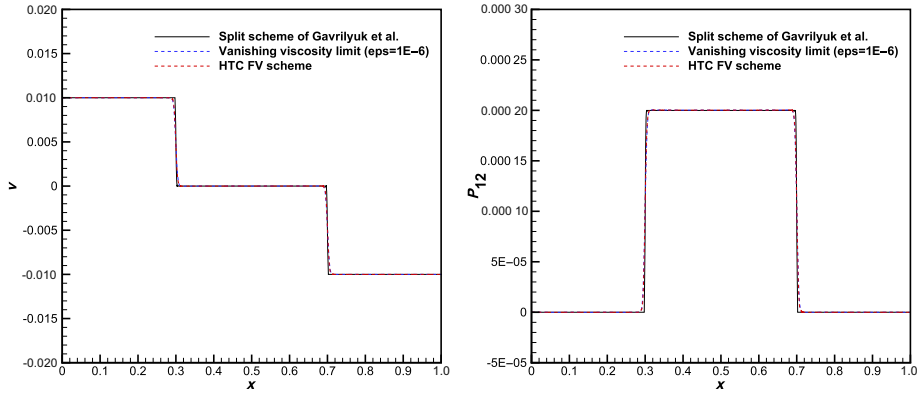

Fig. 17 Turbulent shallow water flow: comparison of the numerical solutions obtained with different methods for Riemann problem RP2 at time $t = 10$: split scheme of [41] on 100 000 elements (solid black line); fourth order ADER-DG scheme ($N = 3$) on 10 200 elements [16] applied to the vanishing viscosity limit of system (21a)–(21d) with viscosity coefficient $\epsilon = 1 \times 10^{-6}$ (dashed blue line); the new thermodynamically compatible HTC FV scheme presented in this paper using 28 000 elements (dashed red line)

4.3.2 Roll Waves

As last test, we consider the one-dimensional roll waves benchmark put forward in [41] from the experimental setup by Brock in [13, 14]. The periodic computational domain $\Omega = [0, 1.3]$ is discretized using 2 000 control volumes. The initial condition reads

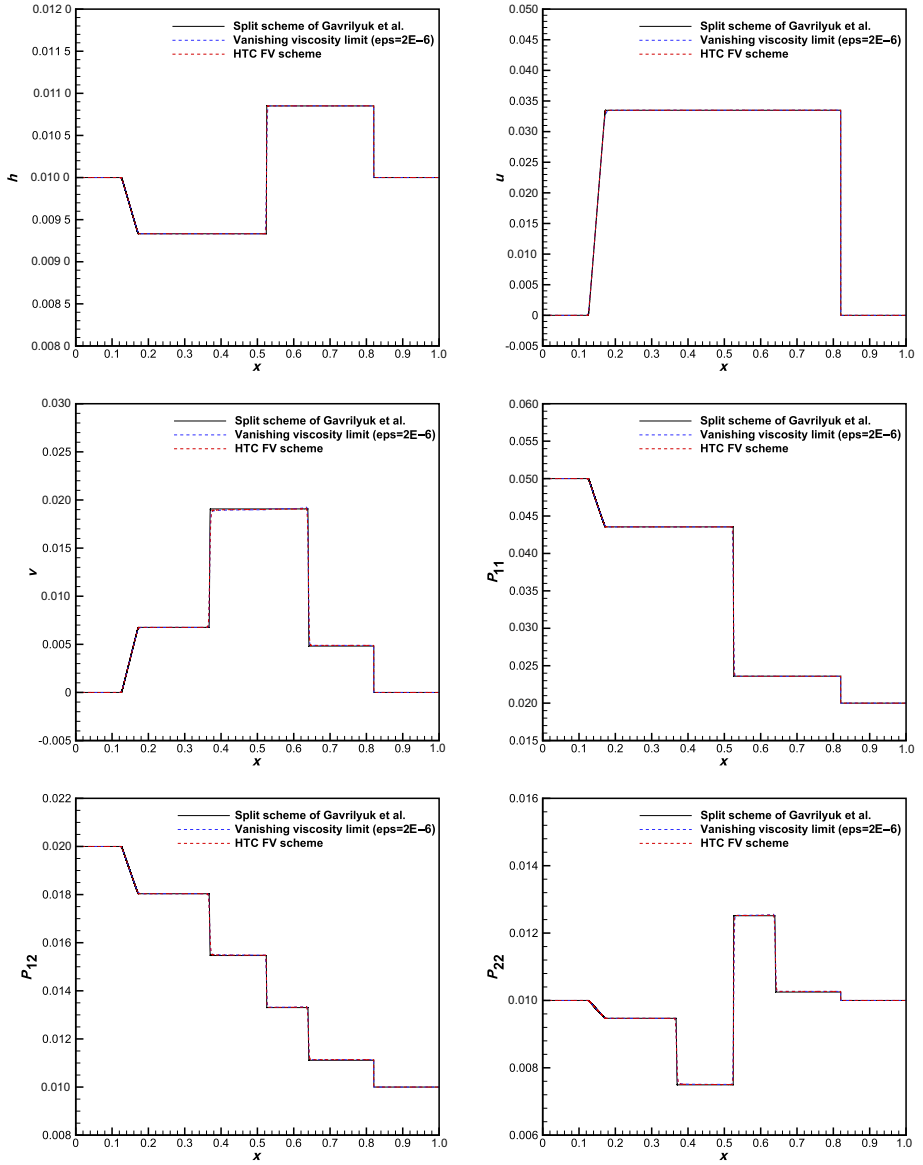

Fig. 18 TSW flow: comparison of the numerical solutions obtained with different methods for Riemann problem RP3 at time $t = 0.5$: split scheme of [41] on 250 000 elements (solid black line); fourth-order ADER-DG scheme ($N = 3$) on 10 200 elements [16] applied to the vanishing viscosity limit of system (21a)–(21d) with the viscosity coefficient $\epsilon = 2 \times 10^{-6}$ (dashed blue line); the new thermodynamically compatible HTC FV scheme presented in this paper using 28 000 elements (dashed red line)

$$h = h_0 \left(1 + a \sin\left(\frac{2\pi}{1.3} x\right)\right), \quad v_1 = \sqrt{\frac{g h_0}{C_f} \tan\theta}, \quad v_2 = 0, \quad \mathbf{Q} = \sqrt{\frac{1}{2}\varphi h^2}\mathbf{I},$$

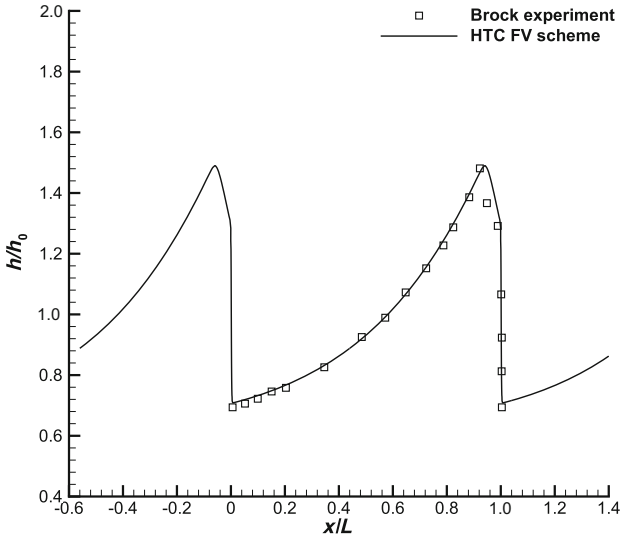

Fig. 19 Comparison of the numerical solution obtained with the new HTC-FV scheme and the experimental data of Brock [13, 14] for the roll wave test problem at time $t = 12.5$

where $a = 0.05$, $\theta = 0.050\ 11$, $h_0 = 0.007\ 98$, $C_f = 0.003\ 6$, $C_r = 0.000\ 35$, and $\varphi = 22.76$. Moreover, we define $\partial_x b = \tan(\theta)$ and the additional source terms $-C_f \sqrt{v_m v_m} v_i$ and $-\frac{\alpha}{h Q_{ik}}$ with $\alpha = \max\left(0, C_r \frac{\mathrm{tr}(\mathbf{P}) - \varphi h^2}{\mathrm{tr}(\mathbf{P}^2)} \|\mathbf{v}\|^3\right)$, must be incorporated at the right-hand side of the momentum equation (21b), see [41] and [16] for details. Due to the dissipative source terms the total energy in the turbulent flow is no longer conserved for this test case. Following [16], the bottom slope is simply implemented as an algebraic source. To complete the problem setup, an artificial viscosity of $\epsilon = 4 \times 10^{-5}$ is set.

The numerical solution obtained with the new HTC-FV scheme is shown in Fig. 19 together with the experimental profile of Brock documented in [13, 14, 41]. As in [16], the spatial coordinate of the numerical results has been normalized by the reference length $L = 1.3$ and the water depth has been normalized by h_0, i.e., we plot $\frac{h}{h_0}$ over $\frac{x}{L}$. The numerical results are reported at the final time $t = 12.5$, i.e., after to two periods of the simulation. Overall, a good agreement is observed between the numerical results and the experimental reference data.

5 Conclusion

We have introduced a very simple, efficient, and general extension of the new family of finite volume schemes based on the thermodynamically compatible Abgrall flux recently presented in Abgrall et al. [3]. Unlike in previous work [3], the new thermodynamically compatible numerical flux (40) with (41) forwarded in this paper also directly takes into account the non-conservative products present in the governing PDE system. In this way, it is no longer necessary to construct a particular thermodynamically compatible discretization of the non-conservative terms case by case and specific for each hyperbolic system, as previously done in [3, 16, 17]. Our new approach is instead totally universal and applies to any overdetermined first-order hyperbolic system of balance laws of the general form (1) that satisfies an extra

conservation law of the type (2). Furthermore, unlike in [16, 17] the numerical flux is not based on path integrals that require expensive and error prone numerical quadrature, but rather relies on a very simple correction based on the jumps in the main field variables.

A key feature of our scheme is that the total energy conservation is obtained as a consequence of the compatible discretization, while entropy-like variables are discretized directly.

In order to show the performance, simplicity and universality of the new numerical method proposed in this paper, we have applied it to three representative overdetermined hyperbolic systems: the augmented equations of ideal MHD with thermodynamically compatible GLM divergence cleaning, the unified first order hyperbolic model of continuum mechanics of the GPR model and the hyperbolic model of TSW flows of Gavrilyuk et al. In all cases, we have observed an excellent agreement between the numerical results obtained with our new method and with available exact, numerical or experimental reference solutions.

Future work will concern the extension to higher order of accuracy in the context of DG finite element schemes, see [3], and the application of the new scheme to the SHTC model of compressible multi-phase flows of Romenski et al. [55, 65, 66, 68, 74]. The particular challenge of the model presented in [65, 66, 68] is the presence of multiple entropy inequalities in the system, but only one scalar total energy conservation law is obtained as a consequence. Such systems cannot be discretized with standard finite volume schemes currently available in the literature, while the new approach presented in this paper can in principle be applied in a straightforward manner to this kind of systems. Furthermore, we also plan to extend our new scheme to an exactly divergence-free and curl-free method, making use of suitable staggered meshes. Last but not least, future work may also include the design of different thermodynamically compatible vanishing viscosity regularizations and their compatible discretization.

Acknowledgements The research presented in this paper was funded by the Spanish Ministry of Science and Innovation under project number PID2021-122625OB-I00 and by the Italian Ministry of Education, University and Research (MIUR) in the frame of the PRIN 2017 project *Innovative numerical methods for evolutionary partial differential equations and applications*, the PRIN 2022 project *High order structure-preserving semi-implicit schemes for hyperbolic equations* and under the *Department of Excellence Initiative* 2023-2027. M.D. is member of INdAM GNCS and was also co-funded by the European Union NextGenerationEU (PNRR, Spoke 7 CN HPC). Views and opinions expressed are however those of the author(s) only and do not necessarily reflect those of the European Union or the European Research Council. Neither the European Union nor the granting authority can be held responsible for them. The authors would like to thank the Leibniz Rechenzentrum (LRZ) in Garching, Germany, for the access to SuperMUC-NG under project pr83no as well as the Spanish Supercomputing Network (RES) under project RES-IM-2022-3-0017 and the CESGA supercomputing center in Santiago de Compostela, Spain, for granting access to FinisTerrae 3. The authors are very grateful to the two anonymous referees for their constructive and insightful comments, which helped to improve the clarity and quality of this paper.

Funding Open access funding provided by Universitá degli Studi di Trento within the CRUI-CARE Agreement.

Data Availability The data can be obtained from the authors on reasonable request.

Compliance with Ethical Standards

Conflict of Interest On behalf of all authors, the corresponding author states that there is no conflict of interest.

References

1. Abgrall, R.: A general framework to construct schemes satisfying additional conservation relations. Application to entropy conservative and entropy dissipative schemes. J. Comput. Phys. **372**, 640–666 (2018)
2. Abgrall, R., Bacigaluppi, P., Tokareva, S.: A high-order nonconservative approach for hyperbolic equations in fluid dynamics. Comput. Fluids **169**, 10–22 (2018)
3. Abgrall, R., Busto, S., Dumbser, M.: A simple and general framework for the construction of thermodynamically compatible schemes for computational fluid and solid mechanics. Appl. Math. Comput. **440**, 127629 (2023)
4. Abgrall, R., Öffner, P., Ranocha, H.: Reinterpretation and extension of entropy correction terms for residual distribution and discontinuous Galerkin schemes: application to structure preserving discretization. J. Comput. Phys. **453**, 110955 (2022)
5. Balsara, D.: Second-order accurate schemes for magnetohydrodynamics with divergence-free reconstruction. Astrophys. J. Suppl. Ser. **151**, 149–184 (2004)
6. Balsara, D.: Multidimensional HLLE Riemann solver: application to Euler and magnetohydrodynamic flows. J. Comput. Phys. **229**, 1970–1993 (2010)
7. Balsara, D., Dumbser, M.: Divergence-free MHD on unstructured meshes using high order finite volume schemes based on multidimensional Riemann solvers. J. Comput. Phys. **299**, 687–715 (2015)
8. Balsara, D., Spicer, D.: A staggered mesh algorithm using high order Godunov fluxes to ensure solenoidal magnetic fields in magnetohydrodynamic simulations. J. Comput. Phys. **149**, 270–292 (1999)
9. Becker, R.: Stosswelle und Detonation. Physik **8**, 321 (1923)
10. Bell, J.B., Coletta, P., Glaz, H.M.: A second-order projection method for the incompressible Navier-Stokes equations. J. Comput. Phys. **85**, 257–283 (1989)
11. Bhole, A., Nkonga, B., Gavrilyuk, S., Ivanova, K.: Fluctuation splitting Riemann solver for a non-conservative modeling of shear shallow water flow. J. Comput. Phys. **392**, 205–226 (2019)
12. Bonnet, A., Luneau, J.: Aérodynamique. Théories de la dynamique des fluides. Cepadues Editions, Toulouse (1989)
13. Brock, R.: Development of roll-wave trains in open channels. J. Hydraul. Div. **95**, 1401–1428 (1969)
14. Brock, R.: Periodic permanent roll waves. J. Hydraul. Div. **96**, 2565–2580 (1970)
15. Busto, S., Dumbser, M.: A new thermodynamically compatible finite volume scheme for magnetohydrodynamics. SIAM J. Numer. Anal. (2023). In press
16. Busto, S., Dumbser, M., Gavrilyuk, S., Ivanova, K.: On thermodynamically compatible finite volume methods and path-conservative ADER discontinuous Galerkin schemes for turbulent shallow water flows. J. Sci. Comput. **88**, 28 (2021)
17. Busto, S., Dumbser, M., Peshkov, I., Romenski, E.: On thermodynamically compatible finite volume schemes for continuum mechanics. SIAM J. Sci. Comput. **44**, A1723–A1751 (2022)
18. Busto, S., Río-Martín, L., Vázquez-Cendón, M.E., Dumbser, M.: A semi-implicit hybrid finite volume/finite element scheme for all Mach number flows on staggered unstructured meshes. Appl. Math. Comput. **402**, 126117 (2021)
19. Castro, M., Gallardo, J., Parés, C.: High-order finite volume schemes based on reconstruction of states for solving hyperbolic systems with nonconservative products. Applications to shallow-water systems. Math. Comput. **75**, 1103–1134 (2006)
20. Castro, M.J., Fjordholm, U.S., Mishra, S., Parés, C.: Entropy conservative and entropy stable schemes for nonconservative hyperbolic systems. SIAM J. Numer. Anal. **51**(3), 1371–1391 (2013)
21. Chan, J., Lin, Y., Warburton, T.: Entropy stable modal discontinuous Galerkin schemes and wall boundary conditions for the compressible Navier-Stokes equations. J. Comput. Phys. **448**, 110723 (2022)
22. Chan, J., Taylor, C.G.: Efficient computation of Jacobian matrices for entropy stable summation-by-parts schemes. J. Comput. Phys. **448**, 110701 (2022)
23. Chandrashekar, P., Klingenberg, C.: Entropy stable finite volume scheme for ideal compressible MHD on 2-D Cartesian meshes. SIAM J. Numer. Anal. **54**(2), 1313–1340 (2016)
24. Chandrashekar, P., Nkonga, B., Meena, A.M., Bhole, A.: A path conservative finite volume method for a shear shallow water model. J. Comput. Phys. **413**, 109457 (2020)

25. Cheng, T., Shu, C.-W.: Entropy stable high order discontinuous Galerkin methods with suitable quadrature rules for hyperbolic conservation laws. J. Comput. Phys. **345**, 427–461 (2017)
26. Dedner, A., Kemm, F., Kröner, D., Munz, C.D., Schnitzer, T., Wesenberg, M.: Hyperbolic divergence cleaning for the MHD equations. J. Comput. Phys. **175**, 645–673 (2002)
27. Derigs, D., Winters, A.R., Gassner, G., Walch, S., Bohm, M.: Ideal GLM-MHD: about the entropy consistent nine-wave magnetic field divergence diminishing ideal magnetohydrodynamics equations. J. Comput. Phys. **364**, 420–467 (2018)
28. Dhaouadi, F., Dumbser, M.: A first order hyperbolic reformulation of the Navier-Stokes-Korteweg system based on the GPR model and an augmented Lagrangian approach. J. Comput. Phys. **470**, 111544 (2022)
29. Dhaouadi, F., Favrie, N., Gavrilyuk, S.: Extended Lagrangian approach for the defocusing nonlinear Schrödinger equation. Stud. Appl. Math. **142**, 336–358 (2019)
30. Dumbser, M., Peshkov, I., Romenski, E., Zanotti, O.: High order ADER schemes for a unified first order hyperbolic formulation of continuum mechanics: viscous heat-conducting fluids and elastic solids. J. Comput. Phys. **314**, 824–862 (2016)
31. Falle, S.A.E.G.: Rarefaction shocks, shock errors and low order of accuracy in ZEUS. Astrophys. J. **577**, L123–L126 (2002)
32. Falle, S.A.E.G., Komissarov, S.: On the inadmissibility of non-evolutionary shocks. J. Plasma Phys. **65**, 29–58 (2001)
33. Favrie, N., Gavrilyuk, S.: A rapid numerical method for solving Serre-Green-Naghdi equations describing long free surface gravity waves. Nonlinearity **30**, 2718–2736 (2017)
34. Fjordholm, U.S., Mishra, S.: Accurate numerical discretizations of non-conservative hyperbolic systems. ESAIM Math. Model. Numer. Anal. **46**(1), 187–206 (2012)
35. Fjordholm, U.S., Mishra, S., Tadmor, E.: Arbitrarily high-order accurate entropy stable essentially nonoscillatory schemes for systems of conservation laws. SIAM J. Numer. Anal. **50**(2), 544–573 (2012)
36. Freistühler, H.: Relativistic barotropic fluids: a Godunov-Boillat formulation for their dynamics and a discussion of two special classes. Arch. Ration. Mech. Anal. **232**, 473–488 (2019)
37. Friedrichs, K.: Symmetric positive linear differential equations. Comm. Pure Appl. Math. **11**, 333–418 (1958)
38. Friedrichs, K., Lax, P.: Systems of conservation equations with a convex extension. Proc. Nat. Acad. Sci. USA **68**, 1686–1688 (1971)
39. Gaburro, E., Öffner, P., Ricchiuto, M., Torlo, D.: High order entropy preserving ADER-DG schemes. Appl. Math. Comput. **440**, 127644 (2022)
40. Gassner, G., Winters, A., Kopriva, D.: A well balanced and entropy conservative discontinuous Galerkin spectral element method for the shallow water equations. Appl. Math. Comput. **272**, 291–308 (2016)
41. Gavrilyuk, S., Ivanova, K., Favrie, N.: Multi-dimensional shear shallow water flows: problems and solutions. J. Comput. Phys. **366**, 252–280 (2018)
42. Ghia, U., Ghia, K.N., Shin, C.T.: High-*Re* solutions for incompressible flow using Navier-Stokes equations and multigrid method. J. Comput. Phys. **48**, 387–411 (1982)
43. Godunov, S.K.: An interesting class of quasilinear systems. Dokl. Akad. Nauk **139**(3), 521–523 (1961)
44. Godunov, S.K.: Symmetric form of the equations of magnetohydrodynamics. Numer. Methods Mech. Contin. Media. **3**(1), 26–31 (1972)
45. Godunov, S.K.: Thermodynamic formalization of the fluid dynamics equations for a charged dielectric in an electromagnetic field. Comput. Math. Math. Phys. **52**, 787–799 (2012)
46. Godunov, S.K., Romenski, E.: Nonstationary equations of the nonlinear theory of elasticity in Euler coordinates. J. Appl. Mech. Tech. Phys. **13**, 868–885 (1972)
47. Godunov, S.K., Romenski, E.I.: Elements of Continuum Mechanics and Conservation Laws. Kluwer Academic/Plenum Publishers, New York (2003)
48. Guermond, J., Popov, P.: Viscous regularization of the Euler equations and entropy principles. SIAM J. Appl. Math. **74**, 284–305 (2014)
49. Hennemann, S., Rueda-Ramírez, A.M., Hindenlang, F.J., Gassner, G.J.: A provably entropy stable subcell shock capturing approach for high order split form DG for the compressible Euler equations. J. Comput. Phys. **426**, 109935 (2021)
50. Hiltebrand, A., Mishra, S.: Entropy stable shock capturing space-time discontinuous Galerkin schemes for systems of conservation laws. Numer. Math. **126**(1), 103–151 (2014)
51. Hu, C., Shu, C.-W.: Weighted essentially non-oscillatory schemes on triangular meshes. J. Comput. Phys. **150**, 97–127 (1999)
52. Ivanova, K., Gavrilyuk, S.: Structure of the hydraulic jump in convergent radial flows. J. Fluid Mech. **860**, 441–464 (2019)
53. Jiang, G., Wu, C.: A high-order WENO finite difference scheme for the equations of ideal magnetohydrodynamics. J. Comput. Phys. **150**, 561–594 (1999)

54. Liu, Y., Shu, C.-W., Zhang, M.: Entropy stable high order discontinuous Galerkin methods for ideal compressible MHD on structured meshes. J. Comput. Phys. **354**, 163–178 (2018)
55. Lukácová-Medvidóvá, M., Puppo, G., Thomann, A.: An all Mach number finite volume method for isentropic two-phase flow. J. Numer. Math. (2022)
56. Munz, C., Omnes, P., Schneider, R., Sonnendrücker, E., Voss, U.: Divergence correction techniques for maxwell solvers based on a hyperbolic model. J. Comput. Phys. **161**, 484–511 (2000)
57. Nkonga, B., Chandrashekar, P.: Exact solution for Riemann problems of the shear shallow water model. ESAIM Math. Modell. Numer. Anal. **56**(4), 1115–1150 (2022)
58. Parés, C.: Numerical methods for nonconservative hyperbolic systems: a theoretical framework. SIAM J. Numer. Anal. **44**, 300–321 (2006)
59. Peshkov, I., Pavelka, M., Romenski, E., Grmela, M.: Continuum mechanics and thermodynamics in the Hamilton and the Godunov-type formulations. Contin. Mech. Thermodyn. **30**(6), 1343–1378 (2018)
60. Peshkov, I., Romenski, E.: A hyperbolic model for viscous Newtonian flows. Contin. Mech. Thermodyn. **28**, 85–104 (2016)
61. Peshkov, I., Romenski, E., Dumbser, M.: Continuum mechanics with torsion. Contin. Mech. Thermodyn. **31**, 1517–1541 (2019)
62. Ray, D., Chandrashekar, P.: An entropy stable finite volume scheme for the two dimensional Navier-Stokes equations on triangular grids. Appl. Math. Comput. **314**, 257–286 (2017)
63. Ray, D., Chandrashekar, P., Fjordholm, U.S., Mishra, S.: Entropy stable scheme on two-dimensional unstructured grids for Euler equations. Commun. Comput. Phys. **19**(5), 1111–1140 (2016)
64. Romenski, E.: Hyperbolic systems of thermodynamically compatible conservation laws in continuum mechanics. Math. Comput. Modell. **28**(10), 115–130 (1998)
65. Romenski, E., Belozerov, A., Peshkov, I.: Conservative formulation for compressible multiphase flows. Q. Appl. Math. **74**, 113–136 (2016)
66. Romenski, E., Drikakis, D., Toro, E.: Conservative models and numerical methods for compressible two-phase flow. J. Sci. Comput. **42**, 68–95 (2010)
67. Romenski, E., Peshkov, I., Dumbser, M., Fambri, F.: A new continuum model for general relativistic viscous heat-conducting media. Philos. Trans. R. Soc. A **378**, 20190175 (2020)
68. Romenski, E., Resnyansky, A., Toro, E.: Conservative hyperbolic formulation for compressible two-phase flow with different phase pressures and temperatures. Q. Appl. Math. **65**, 259–279 (2007)
69. Rueda-Ramírez, A.M., Hennemann, S., Hindenlang, F.J., Winters, A.R., Gassner, G.J.: An entropy stable nodal discontinuous Galerkin method for the resistive MHD equations. Part II: subcell finite volume shock capturing. J. Comput. Phys. **444** (2021)
70. Ruggeri, T., Strumia, A.: Main field and convex covariant density for quasilinear hyperbolic systems Relativistic fluid dynamics. Ann. Inst. Henri Poincaré **34** 65–84 (1981)
71. Schnücke, G., Krais, N., Bolemann, T., Gassner, G.J.: Entropy stable discontinuous Galerkin schemes on moving meshes for hyperbolic conservation laws. J. Sci. Comput. **82**, 69 (2020)
72. Tadmor, E.: The numerical viscosity of entropy stable schemes for systems of conservation laws I. Math. Comput. **49**, 91–103 (1987)
73. Tavelli, M., Dumbser, M.: A pressure-based semi-implicit space-time discontinuous Galerkin method on staggered unstructured meshes for the solution of the compressible Navier-Stokes equations at all Mach numbers. J. Comput. Phys. **341**, 341–376 (2017)
74. Thein, F., Romenski, E., Dumbser, M.: Exact and numerical solutions of the Riemann problem for a conservative model of compressible two-phase flows. J. Sci. Comput. **93**, 83 (2022)
75. Toro, E.: Riemann Solvers and Numerical Methods for Fluid Dynamics. Springer, Cham (2009)